Circulation

ORIGINAL RESEARCH ARTICLE

Nicotinamide Riboside Preserves Cardiac Function in a Mouse Model of Dilated Cardiomyopathy

Editorial, see p 2274

Nicolas Diguet, PhD
Samuel A.J. Trammell, PhD
Cynthia Tannous, PhD*
Robin Deloux, MSc*
Jérôme Piquereau, PhD
Nathalie Mougenot, PhD
Anne Gouge, MSc
Mélanie Gressette, MSc
Boris Manoury, PhD
Jocelyne Blanc, MSc
Marie Breton, MD
Jean-François Decaux, PhD
Gareth G. Lavery, PhD
István Baczkó, MD, PhD
Joffrey Zoll, PhD
Anne Garnier, PhD
Zhenlin Li, PhD
Charles Brenner, PhD
Mathias Mericskay, PhD

BACKGROUND: Myocardial metabolic impairment is a major feature in chronic heart failure. As the major coenzyme in fuel oxidation and oxidative phosphorylation and a substrate for enzymes signaling energy stress and oxidative stress response, nicotinamide adenine dinucleotide (NAD^+) is emerging as a metabolic target in a number of diseases including heart failure. Little is known on the mechanisms regulating homeostasis of NAD^+ in the failing heart.

METHODS: To explore possible alterations of NAD^+ homeostasis in the failing heart, we quantified the expression of NAD^+ biosynthetic enzymes in the human failing heart and in the heart of a mouse model of dilated cardiomyopathy (DCM) triggered by Serum Response Factor transcription factor depletion in the heart (SRF^{HKO}) or of cardiac hypertrophy triggered by transverse aorta constriction. We studied the impact of NAD^+ precursor supplementation on cardiac function in both mouse models.

RESULTS: We observed a 30% loss in levels of NAD^+ in the murine failing heart of both DCM and transverse aorta constriction mice that was accompanied by a decrease in expression of the nicotinamide phosphoribosyltransferase enzyme that recycles the nicotinamide precursor, whereas the nicotinamide riboside kinase 2 (NMRK2) that phosphorylates the nicotinamide riboside precursor is increased, to a higher level in the DCM (40-fold) than in transverse aorta constriction (4-fold). This shift was also observed in human failing heart biopsies in comparison with nonfailing controls. We show that the *Nmrk2* gene is an AMP-activated protein kinase and peroxisome proliferator-activated receptor α responsive gene that is activated by energy stress and NAD^+ depletion in isolated rat cardiomyocytes. Nicotinamide riboside efficiently rescues NAD^+ synthesis in response to FK866-mediated inhibition of nicotinamide phosphoribosyltransferase and stimulates glycolysis in cardiomyocytes. Accordingly, we show that nicotinamide riboside supplementation in food attenuates the development of heart failure in mice, more robustly in DCM, and partially after transverse aorta constriction, by stabilizing myocardial NAD^+ levels in the failing heart. Nicotinamide riboside treatment also robustly increases the myocardial levels of 3 metabolites, nicotinic acid adenine dinucleotide, methylnicotinamide, and N1-methyl-4-pyridone-5-carboxamide, that can be used as validation biomarkers for the treatment.

CONCLUSIONS: The data show that nicotinamide riboside, the most energy-efficient among NAD precursors, could be useful for treatment of heart failure, notably in the context of DCM, a disease with few therapeutic options.

*Drs Tannous and Deloux contributed equally.

Key Words: acetyl coenzyme A ■ cardiomyopathy, dilated ■ energy metabolism ■ glycolysis ■ heart failure ■ NAD ■ nicotinamide-beta-riboside ■ serum response factor

Sources of Funding, see page 2271

http://circ.ahajournals.org

Clinical Perspective

What Is New?

- Myocardial nicotinamide adenine dinucleotide (NAD) coenzyme levels are depressed in mouse models of heart failure.
- An expression shift occurs in murine and human failing hearts in which the normally predominant nicotinamide phosphoribosyltransferase enzyme using nicotinamide as a precursor for NAD+ synthesis is repressed, whereas the nicotinamide riboside kinase 2 enzyme using the nucleoside nicotinamide riboside (NR) is strongly upregulated.
- The nicotinamide riboside kinase 2pathway is activated by energy stress in an AMP-activated protein kinase α/peroxisome proliferator-activated receptor α–dependent manner in cardiomyocytes.
- NR-supplemented diet administrated to murine models of dilated cardiomyopathy or pressure overload-induced heart failure restores myocardial NAD levels and preserves cardiac function.
- NR increases glycolysis, and citrate and acetyl-coenzyme A metabolism, as well, in cardiomyocytes.

What Are the Clinical Implications?

- NR is the most energetically favorable NAD precursor and was recently shown to be uniquely and orally bioavailable in humans in a phase I clinical trial.
- NR-supplemented diet could help patients who have heart failure to cope with limited myocardial ATP supply by restoring NAD coenzyme levels and associated signaling.
- NR-supplemented diet has been shown in several studies to enhance metabolic flexibility in the context of obesity and diabetes mellitus and to improve muscle function, justifying that NR is put in the front line for metabolic therapy of heart failure syndrome in which these functions are altered.

Despite progress in therapeutic advances, mortality remains high in congestive heart failure (HF), creating a need for new evidence-based and cost-effective treatments. Failure of cardiomyocyte bioenergetics is a key issue in HF that is not well addressed in current therapeutics.[1,2] We focused our attention on pathways that regulate nicotinamide adenine dinucleotide (NAD+) homeostasis in the failing heart, which has emerged as a new avenue for the development of metabolic therapy of HF.[3,4] NAD+ is the major hydride transfer coenzyme in fuel oxidation and mitochondrial ATP generation and is the precursor for NADPH, which is required for anabolic pathways and reactive oxygen species detoxification.[5,6] In addition, NAD+ is an essential substrate of enzymes including sirtuins and poly(ADP-ribose) polymerases, which are important in responding to altered nutritional status and genotoxic stress.[6,7] Sirtuins perform NAD+-dependent deacylation of protein Lys residues modified by acetyl coenzyme A (Ac-CoA) derived acyl groups.[8] Sirtuins regulate nuclear gene expression, and mitochondrial enzyme activities, as well, and can play a protective role in the heart,[9] although chronic overactivation may be deleterious.[10] Poly(ADP-ribose) polymerase 1 is activated by reactive oxygen species–induced DNA lesions, and could deplete myocardial NAD+ stores in HF.[11] In situations of physiological equilibrium, biosynthetic pathways relying on dietary sources of tryptophan and NAD+ precursor vitamins counterbalance the consumption of NAD+ by signaling enzymes. However, dietary precursors may become insufficient to maintain the NAD+ metabolome in pathological conditions, thereby necessitating supplementation of NAD+ precursor.[5,12,13]

The homeostasis of NAD+ and regulation of NAD+ biosynthetic enzymes have not been studied in dilated cardiomyopathy (DCM), a leading cause of heart transplant.[14] We previously generated a powerful model of nonischemic DCM in mice triggered by cardiac-specific inducible inactivation of Serum Response Factor (*SRF*^{HKO} model).[15–18] SRF is a major transcriptional regulator of genes and microRNAs involved in contractility, and in energy flux and calcium handling, as well.[15,17,18] The SRF pathway is altered in the human failing heart[19,20] and in animal models of DCM.[21,22] The heart of *SRF*^{HKO} mutant mice display an early downregulation of myofibrillar creatine kinase (CK) activity encoded by the *Ckm* gene, which is followed by repression of enzymes of fatty acid β-oxidation and loss of ATP, thus recapitulating the transitional steps toward energy failure and cardiac structural remodeling in HF.[18]

Here, we show that NAD+ homeostasis is altered at an early stage in the heart of *SRF*^{HKO} mice with a striking induction of the nicotinamide riboside kinase 2 (NMRK2) pathway for NAD+ synthesis. *Nmrk2* gene is 1 of 2 mammalian paralogs of the yeast *NRK1* gene that was discovered as a eukaryotic route to NAD+ from nicotinamide riboside (NR).[23] Given the activity of NR in promoting sirtuin activity and restoring metabolic balance in a variety of model organisms,[13,24–28] we aimed to test whether NR might treat HF in *SRF*^{HKO} mice and in the pressure overload hypertrophy model induced by transverse aorta constriction (TAC). Here, we show that NR greatly protects cardiac function by virtue of improved citrate and Ac-CoA metabolism and antioxidant gene expression. Because NR is orally available in people,[29] our data rationalize clinical testing of NR in human HF.

METHODS

The data, analytic methods, and study materials will be made available from the corresponding author on request to other researchers for purposes of reproducing the results or replicating the procedure. Detailed methods are available in the online-only Data Supplement.

Patients

Left ventricular (LV) myocardium was obtained from terminally failing human hearts of 4 patients (mean age 54 years±7, SD) at the time of transplantation at the Hôpitaux Universitaires de Strasbourg as previously published with approval of the Hôpitaux Universitaires de Strasbourg ethics committee.[30] All patients gave informed consent. Patients' characteristics are detailed in Table I in the online-only Data Supplement. The investigations conformed to the principles of the Declaration of Helsinki. Control hearts were obtained from the department of Pharmacology and Pharmacotherapy, University of Szeged, Szeged, Hungary. Experimental protocols were approved by the Ethical Review Board of the Medical Center of the University of Szeged and by the Scientific and Research Ethical Committee of the Medical Scientific Board at the Hungarian Ministry of Health (ETT-TUKEB; No. 51–57/1997 OEj and 4991-0/2010-1018EKU).

Transgenic Mice

All experiments with animals conformed to the Directive 2010/63/EU of the European Parliament and were approved by the ethics committee Charles Darvin #5 (agreement 00369.01). See online-only Data Supplement for details on SRF inactivation protocol.

NR Supplementation

SRF^{HKO} and control (*Sf/Sf*) mice were administered A04 rodent maintenance diet (Scientific Animal Food Engineering) supplemented with NR chloride provided by Chromadex. See online-only Data Supplement for details.

Transcriptomic Analysis

Transcriptomic data are available on NCBI Gene Expression Database, Accession number GSE84142.

Statistical Analysis

Animals were randomly assigned into different treatment groups. To assess significance, we performed Student *t* test for independent samples when the experimental design compared only 2 groups, or 1-way ANOVA for multiple group comparisons, or 2-way factorial ANOVA for independent factors when appropriate. Tukey tests were used for comparison of specific experimental groups when 1-way ANOVA gave a *P* value of <0.05 or, in the case of 2-way ANOVA for interaction, a *P* value of <0.05. Values are expressed as mean±SEM.

Supplemental Information

Supplemental information includes supplemental methods, 9 supplemental figures, and 6 supplemental tables.

RESULTS

NMRK2 Pathway Is Activated in the Failing Heart of *SRF*^{HKO} Mice

Transcriptome analyses in *SRF*^{HKO} mice at baseline or after phenylephrine α-adrenergic stimulation[16] revealed that the *Nmrk2* gene was induced at an early stage in the *SRF*^{HKO} heart and rose continuously during establishment of HF (Figure 1A and Table II in the online-only Data Supplement). The transcript for the ectoenzyme NT5E (CD73) that hydrolyzes extracellular NAD$^+$ and nicotinamide mononucleotide (NMN) to NR, the substrate of NMRK2 kinase[31] also increased in *SRF*^{HKO} hearts (Table II in the online-only Data Supplement). In contrast, the transcripts encoding nicotinamide phosphoribosyltransferase (NAMPT), the enzyme converting nicotinamide (NAM) to NMN, and purine nucleoside phosphorylase (PNP), which converts NR to NAM,[32] were depressed on phenylephrine treatment in *SRF*^{HKO} hearts (Table II in the online-only Data Supplement). Genes involved in the tryptophan and nicotinic acid pathways for NAD$^+$ synthesis were not altered (Figure 1A and Table II in the online-only Data Supplement).

Modulation of *Nmrk2* and *Nampt* gene expression detected by transcriptomics was corroborated at the mRNA and protein level (Figure 1B through 1D). We observed a similar shift in human patients from predominant expression of NAMPT in healthy hearts to increased NMRK2 and depressed NAMPT in failing hearts (Figure 1D, Table II in the online-only Data Supplement). In mouse heart sections, NMRK2 protein localizes at the proximity of sarcolemma in controls (Figure 1E). The signal was strongly enhanced and spread to cytoplasm in *SRF*^{HKO} cardiomyocytes.

At day 15 after SRF inactivation, there was a 30% loss of NAD (representing the sum of NAD$^+$ and NADH) (Figure 1F, see Methods in the online-only Data Supplement for details). The gene expression pattern (*Nt5e* and *Nmrk2* up with *Pnp* and *Nampt* down) suggested that cardiac tissue is attempting to mobilize and utilize NR as an NAD$^+$ precursor while not increasing NAM usage. We tested this hypothesis by intraperitoneal administration of NR and NAM to *SRF*^{HKO} mice from day 8 to 15. Consistent with this hypothesis, myocardial NAD levels were preserved by NR but not by NAM (Figure 1F). *Srf* and *Nmrk2* expression levels were not changed by these treatments (Figure 1G and 1H). Because NR is orally available,[26,29] we tested an NR-supplemented diet for 2 weeks. Myocardial NAD levels were reduced in this second series of *SRF*^{HKO} mice in comparison with controls and rescued by NR administration (Figure 1I).

NR Preserves Cardiac Function in the *SRF*^{HKO} Heart

We hypothesized that NR supplementation of food might be beneficial for cardiac function in the context of DCM. We fed control and mutant *SRF*^{HKO} mice a standard chow diet or NR-supplemented diet to reach a dose of 400 mg/kg of body weight per day from day 5 to 50, a period in which untreated *SRF*^{HKO} mice develop DCM and progress toward HF.[15–18] NR diet induced a

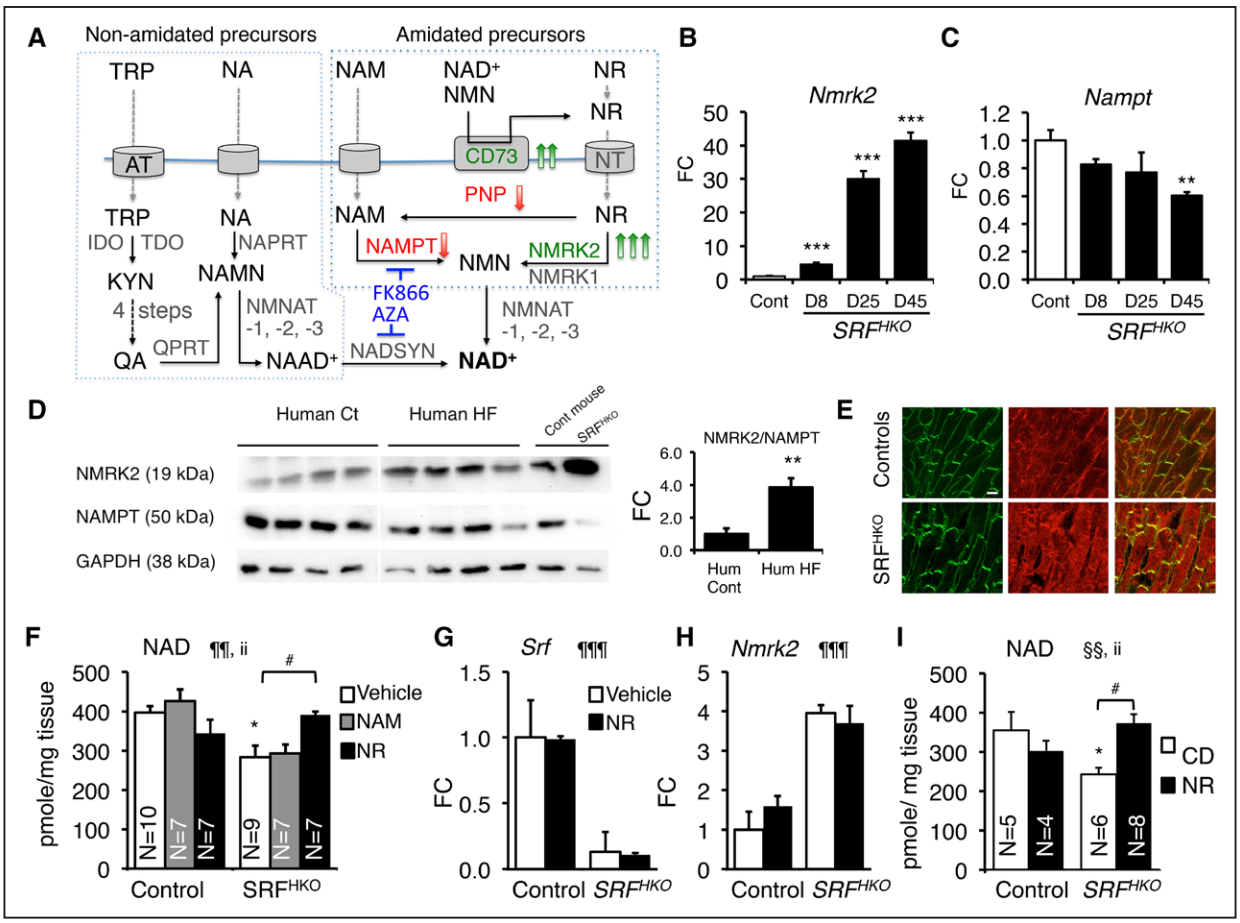

Figure 1. Activation of the *Nmrk2* gene in dilated cardiomyopathy.

A, Biosynthetic NAD+ pathways in mammalian cells. NA (nicotinic acid), NAM, NR, and TRP enter cells through specialized transport systems. Extracellular NAD+ and NMN are hydrolyzed to NR by the ectonucleotidase CD73. In the de novo pathway, TRP is converted to kynurenin (KYN) by IDO and TDO enzymes, and then into quinolic acid (QA) in 4 steps (not detailed). QA, NA, and NAM are phosphoribosylated by QPRT, NAPRT1, and NAMPT enzymes, respectively, to form mononucleotides NAMN and NMN. NR is phosphorylated by NMRK enzymes to form NMN. NR can be converted to NAM by PNP. NAMN and NMN are adenylated by the NMNAT enzymes to form the dinucleotides NAAD+ and NAD+. NAAD+ is amidated by NADSYN1. Genes increased in *SRF*^{HKO} heart are highlighted in green and those repressed in red (see accompanying Table II in the online-only Data Supplement). Inhibitors are shown in blue. **B** and **C,** RT qPCR analysis of *Nmrk2* and *Nampt* mRNA fold change (FC) in *SRF*^{HKO} hearts at different days (D) after SRF inactivation. **D,** Western blot analysis of NMRK2 and NAMPT protein in control and failing human hearts and control and *SRF*^{HKO} mouse hearts at D45. GAPDH is used as loading control. All human and mouse samples were analyzed on single blot, but 2 lanes separating that showed signs of protein degradation and aberrant migration pattern were cut out of the picture. **Right,** Ratio of NMRK2/NAMPT in human samples. **E,** Control and *SRF*^{HKO} mutant heart sections stained for NMRK2 (red) and vinculin (green) at D45. White bar in upper left panel=20 µm. **F** through **H,** NAM or NR (30 µmol) were injected intraperitoneally from D8 to 15 (400 mg/kg per day) to control and *SRF*^{HKO} mice. Vehicle: saline solution. **F**, Myocardial NAD+ levels. **G** and **H**, RT qPCR analysis of *Srf* and *Nmrk2* mRNA levels. **I,** Myocardial NAD levels in control and *SRF*^{HKO} mice fed regular chow diet (CD) or NR-enriched diet (0.22%. 400–450 mg/kg per day) from D5 to 20. Throughout the figure, data are expressed as mean±SEM. Statistical analysis: One-way ANOVA (**B**, **C**) or 2-way factorial ANOVA for independent samples (**F** through **I**). ¶¶P≤0.01, ¶¶¶P≤0.001 for the genotype effect; §§P≤0.01 for the NR treatment effect; ii P≤0.01 for the interaction effect. Post hoc Tukey test: asterisks indicate statistical significant difference between any group versus the control CD (or vehicle) group: *P≤0.05. **P≤0.01. ***P≤0.001. # P≤0.05 for the effect of NR within the *SRF*^{HKO} group. A *t* test was used for the graph at the right of **D**: ** P≤0.01. FC indicates fold change over control group; IDO, indoleamine 2,3-dioxygenase; NAAD, nicotinic acid adenine dinucleotide; NAD, nicotinamide adenine dinucleotide; NAM, nicotinamide; NAMN, nicotinic acid mononucleotide; NAMPT, nicotinamide phosphoribosyltransferase; NMN, nicotinamide mononucleotide; NMNAT, nicotinamide mononucleotide adenylyltransferease; NMRK, nicotinamide riboside kinase; NR, nicotinamide riboside; PNP, purine nucleoside phosphorylase; QPRT, quinolinate phosphoribosyltransferase; RT qPCR, quantitative reverse transcription polymerase chain reaction; SRF, Serum Response Factor; TDO, tryptophan 2,3-dioxygenase; and TRP, tryptophan.

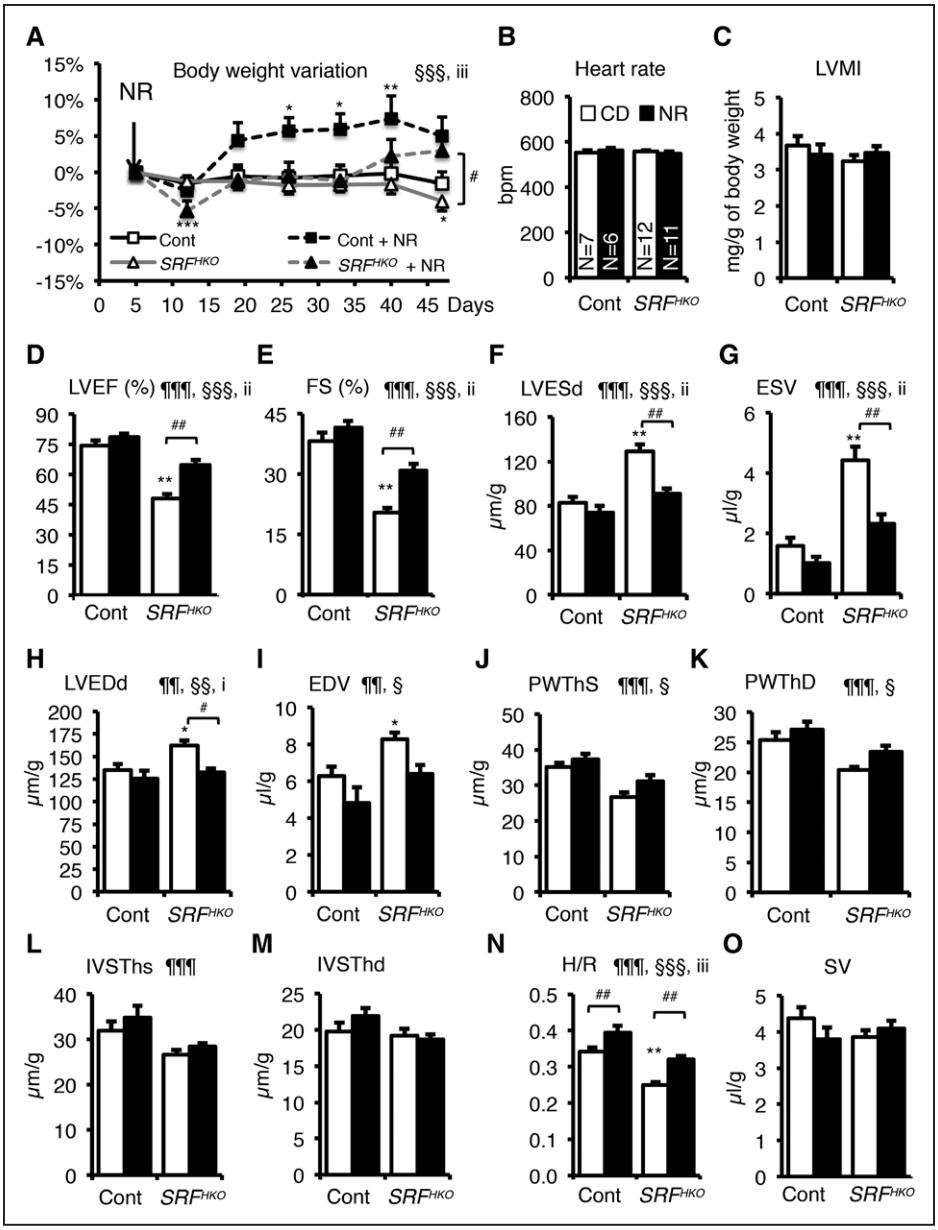

Figure 2. NR supplementation in diet prevents the onset of heart failure and dilatation.
A, CD- or NR-supplemented diet (0.22%) was given ad libitum to control and *SRF*^{HKO} mice from day 5 after SRF inactivation to the end of the experiment. Body weight was monitored throughout the period. Data are expressed as mean % weight variation±SEM, in comparison with weight at day 5. A 2-factor ANOVA with repeated measures on 1 factor was used for statistical analysis. §§§P≤0.001 for the time effect; iii, P≤0.001 for the interaction effect. Post hoc Tukey test: *P<0.05, **P<0.01, ***P<0.001 for any time point versus day 5 within a group; $^{\#}P$≤0.05 for the NR treatment in *SRF*^{HKO} group. **B** through **O,** Cardiac parameters of control and *SRF*^{HKO} mutant were analyzed in M-Mode echocardiography between day 45 and day 47. **B,** Heart rate; **C,** left ventricle (LV) mass index; **D,** LV ejection fraction; **E,** fractional shortening; **F** and **G,** LV end-systolic diameter (**F**) and volume (**G**); **H** and **I,** LV end-diastolic diameter (**H**) and volume (**I**); **J** and **K,** LV posterior wall thickness in systole (**J**) and diastole (**K**); **L** and **M** interventricular septum thickness in systole (**L**) and diastole (**M**); **N,** H/R: LV thickness (H) to radius (R) ratio; and **O,** stroke volume. Dimensions were normalized by the body weight. Data are expressed as mean±SEM. Statistical analysis: 2-way factorial ANOVA for independent samples. ¶¶P≤0.01, ¶¶¶P≤0.001 for the genotype effect; §P≤0.05, §§P≤0.01, §§§P≤0.001 for the NR treatment effect; i P≤0.05, ii P≤0.01, iii P≤0.001 for the interaction effect. Post hoc Tukey test: asterisks indicate statistically significant difference versus the control CD group: *P≤0.05, **P≤0.01, ***P≤0.001. #P≤0.05, ##P≤0.01 for the effect of NR within the *SRF*^{HKO} group. CD indicates chow diet; CONT, control; EDV, end-diastolic volume; ESV, end-systolic volume; FS, fractional shortening; IVSThd, interventricular septum thickness in diastole; IVSThs, interventricular septum thickness in systole; LVEF, left ventricular ejection fraction; LVEDd, left ventricular end-diastolic diameter; LVESd, left ventricular end-systolic diameter; LVMI, left ventricular mass index; NR, nicotinamide riboside; PWThD, posterior wall thickness in diastole; PWThS, posterior wall thickness in systole; and SV, stroke volume.

modest 5% to 7% increase in body weight in control mice and allowed *SRF*^{HKO} mice to regain weight after an initial loss, whereas *SRF*^{HKO} mice on a regular diet had lost weight at the end of the protocol (Figure 2A). Cardiac parameters were analyzed by echocardiography between days 45 and 47 (Figure 2B through 2O). NR did not change heart rate and LV mass index, but slightly it increased the LV thickness-to-radius ratio (H/R) in control mice (Figure 2N). To assess a potential impact of NR treatment on vascular function, we compared vascular reactivity in isolated mesenteric arteries from NR-fed and control mice. We found no difference between the 2 groups neither in responses to K^+ or agonist-induced contraction nor in the relaxation response to carbachol or a NO donor (Figure I in the online-only Data Supplement and Table III in the online-only Data Supplement).

SRF^{HKO} mutant mice fed the standard diet displayed a severe decrease in LV ejection fraction and fractional shortening (Figure 2D and 2E). The NR diet clearly protected against this decline in cardiac function. It is important to note that NR fully protected *SRF*^{HKO} mice against the dilatation and thinning of the LV wall (Figure 2F through 2M), preserving the H/R ratio that normally declines with DCM (Figure 2N). Changes in stroke volume (Figure 2O) and cardiac output (not shown) were not significant.

At the histological level, NR limited the appearance of very long cardiomyocytes (Feret > 100 µm) in *SRF*^{HKO} mice, although the population of large cardiomyocytes (minFeret > 26 µm) remained larger than in controls (Figure II in the online-only Data Supplement).

NR-Enriched Diet Protects the Cardiac NAD$^+$ Metabolome in HF

The impact of an NR-enriched diet on the cardiac NAD$^+$ metabolome is not known (Figure 3A). Mice fed with or without NR were euthanized 3 days after the echocardiography at day 50. Myocardial NAD was decreased in the *SRF*^{HKO} mice at day 50 as measured by the NAD cycling assay, and the NR diet protected against this drop (Figure 3B). Myocardial NAD$^+$ and NADH varied in the same direction in all conditions, leaving the NAD$^+$/NADH ratio unchanged (Figure III in the online-only Data Supplement). Liquid chromatography-mass spectrometry analysis allowed us to provide the levels of NAD$^+$ metabolites on a common scale with NAD$^+$[13,33] (Figure 3C through 3L). *SRF*^{HKO} mice hearts did not have higher levels of adenosine diphosphate ribose (ADPR) or NAM (Figure 3D and 3E). Levels of NADP$^+$ and NMN showed a pattern similar to NAD$^+$ (Figure 3F and 3G).

NR increased the cardiac levels of nicotinic acid adenine dinucleotide, a sensitive biomarker of increased NAD$^+$ metabolism,[29] and methyl-NAM (MeNAM), as well (Figure 3A, 3H through 3J). MeNAM oxidation by AOX1 generates N1-methyl-4-pyridone-5-carboxamide (Me4PY) and releases hydrogen peroxide (Figure 3A). Changes in unrelated metabolites were not significant (Figure 3K and 3L). As shown in the nematode,[34] NR increased the expression of the *Nfel2* gene encoding NRF2, whereas its target genes *Mt2* and *Nox4* were already activated, and *G6pdx*, as well, in the heart of *SRF*^{HKO} mice (Figure 3M through 3P). NR treatment in the *SRF*^{HK0} hearts limited the level of *Myh7* induction, a signature of cardiac stress and metabolic remodeling in the failing heart (Figure 3Q).

The liver is a central organ for the regulation of nutrient metabolism. We assessed the NAD$^+$ metabolome response in the liver of control and *SRF*^{HKO} mice (Table IV in the online-only Data Supplement). NR increased the MeNAM and Me4PY levels similarly in both genotypes. It is interesting to note that the liver response to NR diet was more robust in the *SRF*^{HKO} mice with regard to the increase in the steady-state level of NAD, nicotinic acid adenine dinucleotide, ADPR, and NAM. Because the liver is not targeted by the *Srf* deletion, it suggests that the HF condition indirectly modifies the balance of NAD synthesis and signaling in the liver.

NR-Enriched Diet Does Not Result in Global Cardiac Protein Deacetylation

The cardiac levels of NAM and ADPR in this HF model are low and show few changes with NR (Figure 3D and 3E), suggesting that the NR-driven boost in NAD$^+$ synthesis is not necessarily translated into a higher level of NAD$^+$ consumption by sirtuins and poly(ADP-ribose) polymerases. We performed antiacetyl-K and anti–poly-ADP-ribose Western blot analyses on cardiac proteins from control and *SRF*^{HKO} mice fed with the chow diet or NR-enriched diets. Just as levels of ADPR were not modulated by *SRF*^{HKO} or NR, neither were levels of PAR (Figure IVA in the online-only Data Supplement). There was an increase in the acetylation level of some cardiac proteins in the hearts of NR-fed animals (Figure IVB in the online-only Data Supplement). Antibodies specific to the acetylated form of FOXO1 or p53 showed an increase in the acetylation level of these nuclear proteins in the heart in response to NR in controls as in *SR*^{FHKO} mice (Figure 3R, Figure V in the online-only Data Supplement). By comparison, the acetylation level of the mitochondrial aconitase 2 protein did not change in any of these conditions despite lower protein level in the *SRF*^{HKO} hearts (Figure 3S and Figure VIA in the online-only Data Supplement). These data suggest that the bioenergetic improvement in NR-supplemented hearts may result in greater production of cytosolic Ac-CoA and consequent increased nucleocytosolic protein acetylation.

NR Improves Metabolism of Citrate in HF

Several regulators involved in mitochondrial biogenesis and oxidative metabolism, and lipid metabolism, as

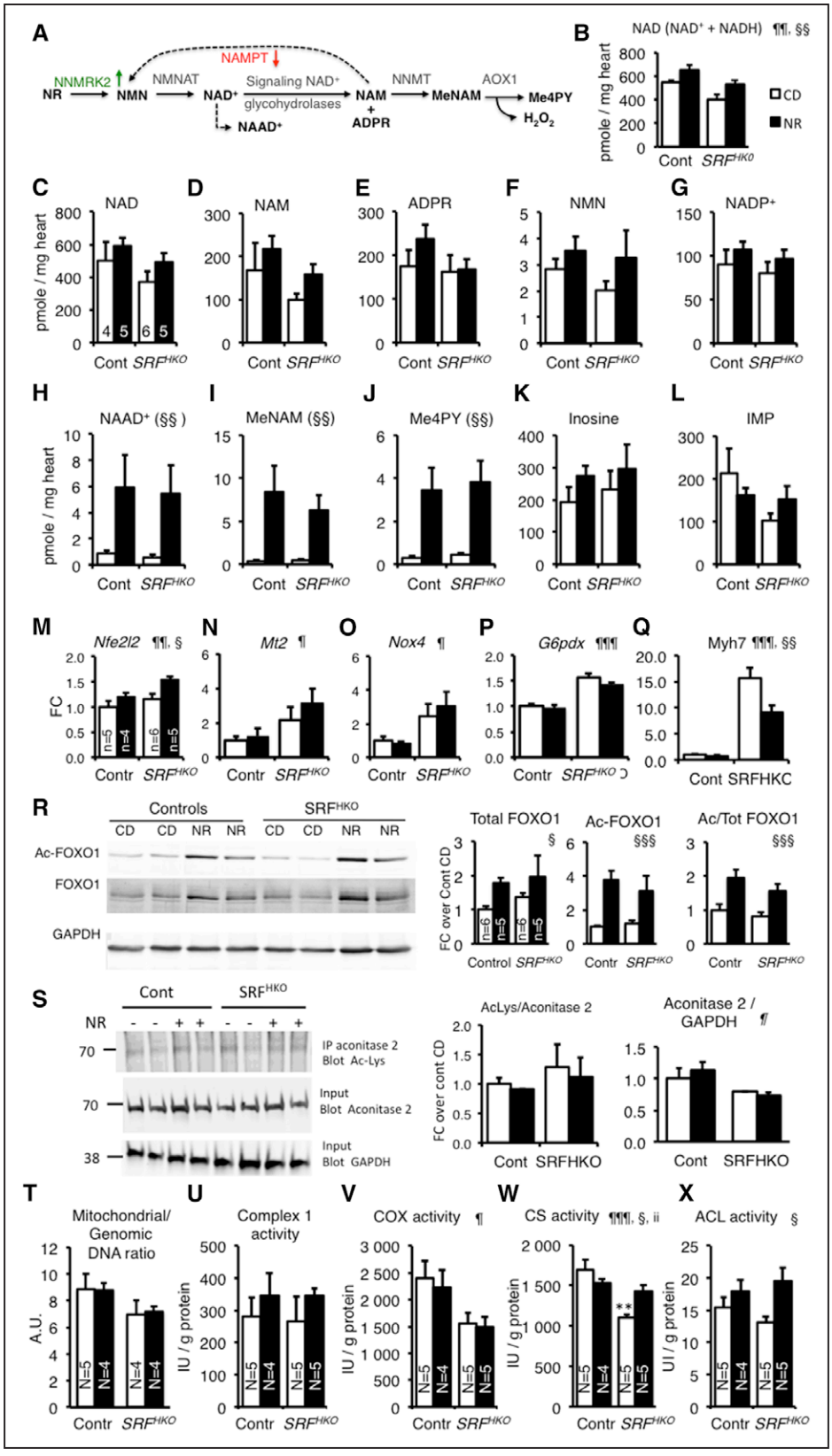

Figure 3. Impact of NR treatment on cardiac NAD⁺ metabolome.

A, NR to NAD⁺ pathway and NAD⁺ catabolism are depicted. NAD⁺ is cleaved into NAM and ADP-ribose by NAD⁺-consuming enzymes. NAM is either recycled by NAMPT or methylated by the nicotinamide *N*-methyltransferase (NNMT) enzyme and oxidized by the aldehyde deoxidase 1 (AOX1) giving rise to degradation products MeNAM and Me4PY, respectively. **B,** Myocardial NAD was quantified by colorimetric NAD⁺ cycling assay at day 50 in controls (n=6), Controls+NR (*Continued*)

well, were repressed in *SRF*^{HKO} hearts (Figure VIIA and VIIB in the online-only Data Supplement). Simultaneously, the expression of the glucose transporter *Glut1* was increased and expression of *Pdk2* was decreased, which can be seen as a trend of the failing heart to increase glycolysis (Figure VIIC in the online-only Data Supplement). NR did not alter the expression of these genes.

There was a trend toward a reduced mitochondrial to genomic DNA ratio in the *SRF*^{HKO} LV (Figure 3T). The NADH-dependent complex I activity and Cox activity was not changed by the NR diet (Figure 3U and 3V). Neither the complex I and II maximal respiration rates, nor the apparent K_m for ADP, mitochondrial CK coupling, and ADP acceptor control ratio showed any alteration at this stage (day 50) in the *SRF*^{HKO} LV fibers. These parameters were not altered by NR administration (Figure VIID through VIIG in the online-only Data Supplement).

We noted that NR treatment resulted in a net increase in acetylation of FOXO1 and p53 (Figure 3R and Figure V in the online-only Data Supplement). Availability of cytosolic Ac-CoA depends on mitochondrial citrate synthase (CS) production of citrate and conversion to Ac-CoA via the cytosolic enzyme, ATP-citrate lyase (ACL). CS activity was reduced to 65% of control levels in the *SRF*^{HKO} LV myocardium (Figure 3W). It is striking that NR administration protected against the decline of CS activity in the failing heart. This rescue in activity occurred despite a net reduction in protein level in the *SRF*^{HKO} myocardium that was not rescued by the NR treatment (Figure VIB in the online-only Data Supplement). It is interesting to that NR also increased cardiac ACL activity in both control and *SRF*^{HKO} mice (Figure 3X). Taken together, these data suggest that NR improves CS and ACL activity, resulting in increased nucleocytoplasmic protein acetylation.

Nmrk2 Gene Is Induced by Inhibition of Alternative NAD$^+$ Biosynthetic Pathways in Cultured Cardiomyocytes

To assess the impact of NMRK2 on NAD$^+$ biosynthesis relative to the other pathways in cardiomyocytes, we used chemical inhibitors to target the alternative pathways in neonatal rat cardiomyocytes (NRCs) grown in Dulbecco modified Eagle medium containing NAM as the vitamin B3. The glutamine analog azaserin inhibits the glutamine-dependent NAD synthase NADSYN1,[35] which catalyzes the last step of NAD$^+$ synthesis from tryptophan and NA (Figure 1A). FK866 is a specific inhibitor of Nampt.[36]

Azaserin had a slowly repressive effect on NAD pools that resulted in a 50% reduction with respect to nontreated cells at 72 hours (Figure 4A through 4C) while progressively increasing *Nmrk2* expression (Figure 4D). FK866 treatment led to a rapid and severe loss of intracellular NAD$^+$ but not NADH (Figure 4A through 4C). Despite this severe loss, NRC could be maintained up to 72 hours in continuous layer with FK866 treatment. FK866 treatment strongly increased *Nmrk2* expression at 72 hours (Figure 4D). Combined azaserin and FK866 treatment had a similar impact than FK866 alone (Figure 4A through 4D). *Nmrk1* expression did not change in these conditions (not shown).

We tested whether NR could preserve NAD$^+$ levels in the presence of FK866. NR slightly increased the baseline level of intracellular NAD$^+$ in nontreated NRC, whereas exogenous NAD$^+$ had no impact (Figure 4E). Both compounds increased the NAD$^+$/NADH ratio (Figure 4F and 4G). NR fully protected NAD$^+$ levels in NRCs treated with FK866, whereas the protection by exogenous NAD$^+$ was partial (Figure 4E), although both treat-

Figure 3 Continued. (n=5), *SRF*^{HKO} (n=6), *SRF*^{HKO}+NR (n=6). Data are expressed as means±SEM. **C** through **L,** Myocardial metabolites were analyzed by LCMS-based metabolomics. See abbreviations in the text. Controls (n=4), controls+NR (n=5), *SRF*^{HKO} (n=6), +NR (n=5, except for NAM, MeNAM, and Me4PY, n=4, no peak was identified in 1 sample). Data are expressed as means±SEM. **M** through **Q,** Expression of genes related to oxidative stress signaling (**M** through **O**) and cardiac structural and metabolic remodeling (**P** and **Q**). n=5 in each group. **R,** Representative Western blot analysis of FOXO1 and acetyl-FOXO1 of 3 independent experiments realized in different duplicates for each group. GAPDH is used as a loading control. **Right graphs,** Quantification of total and acetyl-FOXO1 ratio on GAPDH and acetyl-FOXO1/total FOXO1 ratio in n=5 to 6 animals per group. **S,** Acetylation level of mitochondrial aconitase 2. Aconitase 2 (75 kDa) was immunoprecipitated using a rabbit polyclonal antibody, and the immunoprecipitate was analyzed by Western blot using a mouse monoclonal anti-Ac(K103) antibody. Inputs were run in a parallel gel and immunoblotted with anti-aconitase 2 and anti-GAPDH for loading control. The ratio of acetyl-aconitase2/total aconitase2 and aconitase2/GAPDH are shown (**right**). See accompanying Figure VIA in the online-only Data Supplement for control immunoprecipitation with preimmune rabbit IgG. **T** through **X,** LV cardiac tissue was isolated at 50 days after tamoxifen injection in control and *SRF*^{HKO} mice fed control diet (CD) or NR-enriched diet. DNA and proteins were extracted from parallel samples to quantify mitochondrial to genomic DNA ratio (**T**) and enzymatic activities: complex I (**U**), cytochrome oxidase (**V**), citrate synthase (**W**), and ATP citrate lyase (**X**). See associated Figure VII in the online-only Data Supplement. In **M** through **S**, data are expressed as mean fold change (FC)±SEM over control group CD. Statistical analysis: Two-way factorial ANOVA for independent samples was used for all panels. ¶P≤0.05, ¶¶P≤0.01, ¶¶¶P≤0.001 for the genotype effect; §P≤0.05, §§P≤0.01, §§§P≤0.001 for the NR treatment effect; ii P≤0.01 for the interaction effect. Post hoc Tukey test: asterisks indicate statistically significant difference versus the control CD group: **P≤0.01. ACL indicates ATP-citrate lyase; ADP, adenosine diphosphate ribose; Cont, control; CS, citrate synthase; IMP, inosine monophosphate; LCMS, liquid chromatography-mass spectrometry; NAAD, nicotinic acid adenine dinucleotide; NAD, nicotinamide adenine dinucleotide; NAM, nicotinamide; NAMPT, nicotinamide phosphoribosyltransferase; NMN, nicotinamide mononucleotide; and NR, nicotinamide riboside.

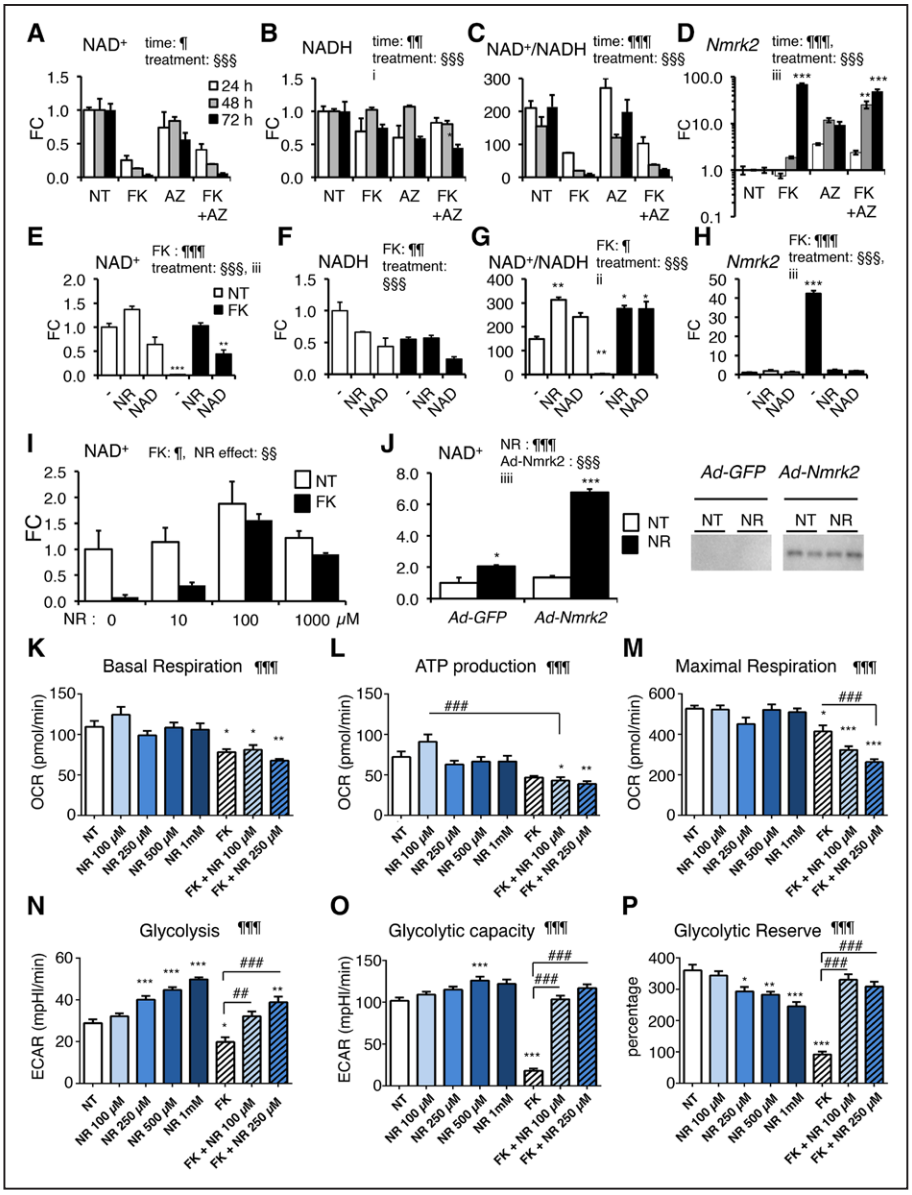

Figure 4. *Nmrk2* expression is activated by repression of alternative NAD⁺ biosynthetic pathways.
A through **C,** Intracellular levels of NAD⁺ (**A**), NADH (**B**), and NAD⁺/NADH ratio (**C**) in NRC after 10 µmol/L FK866 and 20 µmol/L azaserin treatment or no treatment (NT) for 24 to 72 hours as indicated. **D,** *Nmrk2* mRNA level in NRC treated as in **A** through **C**. **E** through **G,** Same as in **A** through **C** in NRC treated for 72 hours with 10 µmol/L FK866 or not treated (NT) in normal culture medium (–) or in presence of 250 µmol/L NAD⁺ or 1 mmol/L NR. **H,** *Nmrk2* mRNA level in NRC treated as in **E** through **G**. **I,** NAD⁺ levels in NRCs treated with 10 µmol/L FK866 for 72 hours, or not treated (NT) in the presence of increasing concentration of NR in culture medium. **J**, NAD⁺ content in nontreated (NT) or following 24-hour NR treatment (1 mmol/L) in NRC infected with Ad-GFP or HA-Nmrk2. **Right,** Western blot detection of HA-NMRK2 with anti-HA antibody. **K** through **M,** Mitochondrial stress test in Seahorse analyzer. NRC grown on Seahorse 96-well plates were analyzed for oxygen consumption rate (OCR) at day 8 after 5 days of treatment. **K**, Basal mitochondrial respiration is calculated from total cellular respiration minus nonmitochondrial respiration. **L**, ATP production is calculated from basal mitochondrial respiration minus respiration after oligomycin injection. **M**, Maximal respiration is measured after FCCP injection. See accompanying Figure IX in the online-only Data Supplement for other respiration parameters. **N** through **P,** Glycolysis stress test in Seahorse analyzer. NRC grown on Seahorse 96-well plates were analyzed at day 8 after 5 days of treatment. **N,** Glycolysis was measured as a function of extracellular acidification rate (ECAR) after injection of 10 mmol/L glucose. **O,** Glycolytic capacity as the maximum ECAR following injection of oligomycin. **P,** Glycolytic reserve as the difference between glycolysis and maximal glycolytic capacity. Throughout the figure, data are expressed as mean fold change (FC)±SEM over the control group, except when indicated. Statistical analysis: a 2-way factorial ANOVA for independent samples was used for **A** through **J**. ¶ and § symbols as indicated in the panels; i $P \leq 0.05$, ii $P \leq 0.01$, iii $P \leq 0.001$ for the interaction effect. One-way ANOVA was used for **K** through **P**. ¶ $P<0.05$, ¶¶ $P<0.01$, ¶¶¶ $P<0.001$. §§ $P \leq 0.01$, §§§ $P \leq 0.001$. Post hoc Tukey test: *$P<0.05$, **$P<0.01$, ***$P<0.001$ between any (*Continued*)

ments blocked *Nmrk2* induction (Figure 4E). At least 100 µmol/L NR was required to rescue the NAD^+ loss induced by 10 µmol/L FK866 (Figure 4I). To assess the functionality of NMRK2 in the absence of a stress like the FK866, we infected NRC with a recombinant adenovirus expressing HA-tagged *Nmrk2* cDNA (Figure 4J). Overexpression of NMRK2 did not modulate the NAD^+ levels in NRC. In presence of NR, *Nmrk2* overexpression robustly increased the NAD^+ level by a factor of 6. NR alone slightly increased the NAD^+ level in control NRC infected with *Ad-GFP* (Figure 4J). In isolated primary cultures of adult rat cardiomyocytes, NR increased intracellular NAD nearly 3-fold, showing that the NMRK pathway is more active in adult rat cardiomyocytes than in NRCs (Figure VIIIA in the online-only Data Supplement). FK866 reduced NAD levels by a factor of 2 (Figure VIIIA in the online-only Data Supplement) in adult rat cardiomyocytes and increased *Nmrk2* expression by a factor of 4.5, whereas azaserin had no impact (Figure VIIIB in the online-only Data Supplement). We assessed the impact of NR on oxygen consumption rates in NRC following a mitochondrial stress protocol. NR had no impact on any mitochondrial respiration parameter in NRC at baseline (Figure 4K through 4M, Figure IX in the online-only Data Supplement). NR increased glycolysis at baseline in a dose-dependent manner (Figure 4N), but not the maximal glycolytic capacity (Figure 4O and 4P**).** We assessed the capacity of NR to rescue any impact of FK866 on metabolism. FK866 reduced basal oxygen consumption rates and maximal respiration and trended to reduce ATP production (adjusted *P* value=0.0547) (Figure 4K through 4M). Addition of NR at doses that we showed to fully rescue the drop in NAD^+ levels triggered by the FK866 did not correct these alterations and even further reduced maximal respiration at high doses (Figure 4K through 4M, Figure IX in the online-only Data Supplement). FK866 strongly reduced basal glycolysis and glycolytic capacities in NRC. NR strikingly preserved NRC glycolytic capacities to 100% control levels and more in FK866-treated cells and stimulated glycolysis at baseline in nontreated cells in a dose-dependent manner (Figure 4N through 4P).

SRF Deficiency-Induced Depression of the *Nmrk2* Promoter Is Counterbalanced by the Sensitivity of *Nmrk2* Gene to NAD^+ Depletion and Energetic Stress

Because *Nmrk2* expression is activated in vivo on *Srf* gene inactivation, we addressed the role of the SRF transcription factor in *Nmrk2* gene regulation. We identified an SRF binding site with 9/10 bp match to the consensus $CC(A/T)_6GG$ (CArG) sequence in a conserved 600-bp region between the murine and human genes (Figure 5A). We cloned the upstream region and 5′-UTR of the murine *Nmrk2* gene (–581/+61) into a luciferase reporter vector and mutated the CArG-like sequence to a motif matching the consensus sequence (5′-CC) or a motif unable to bind SRF (5′-GG) (Figure 5A). FK866 increased the expression of the WT construct 8-fold, whereas a consensus CArG reduced the extent of activation (Figure 5B). The 5′-GG mutation reduced baseline expression by 75% and abolished the response to FK866. The full intergenic 3009-bp sequence upstream of *Nmrk2* had a much higher activity, especially in response to FK866 (Figure 5C). siRNA-mediated inhibition of *Srf* reduced, but did not abolish, the induction of endogenous *Nmrk2* by FK866 in NRC, suggesting that FK866-triggered activation of the *Nmrk2* promoter is partially independent of SRF (Figure 5D and 5E). FK866 treatment reduces ATP to 50% of the control level in NRC (Figure 5F). SRF is major upstream regulator of *Ckm* gene involved in high-energy phosphate compounds balance. A siRNA-mediated 5-fold knock-down of *Ckm* gene expression lowered the cellular ATP levels to 70% control level and triggered a 6.8-fold increase in *Nmrk2* expression (Figure 5G and 5H). A 2-fold reduction in *Srf* expression resulted in a 2-fold reduction of *Ckm* expression leaving *Nmrk2* expression intact. Enforcing a more profound depression of *Ckm* expression in the context of *Srf* repression in NRC by cotransfection with both *Srf* and *Ckm* siRNAs resulted in a 2.3-fold increase in *Nmrk2* expression (Figure 5H).

Nmrk2 Is Induced by the AMPK-PPARα Axis

In line with the previous results, we hypothesized that pathways related to energy failure might activate *Nmrk2*. The level of phosphorylated AMP-activated protein kinase α (AMPKα), the energy stress–sensing AMP-activated kinase, and its target Ac-CoA carboxylase (ACC) was increased at an early stage when *Nmrk2* induction began in the SRF^{HKO} hearts (Figure 6A and 6B). 5-Aminoimidazole-4-carboxamide ribonucleotide (AICAR) treatment stimulated AMPK phosphorylation in NRCs and increased NMRK2 protein level in NRCs (Figure 6C and 6D). The energetic stress induced by glucose deprivation for 24 hours or FK866 for 48 hours also increased the NMRK2 protein.

AICAR treatment did not modulate NAD^+/NADH but robustly induced *Nmrk2* expression (Figure 6E through 6H). To assess whether the effect of AICAR took place at the level of the *Nmrk2* promoter, we transfected *Nmrk2*-

Figure 4 Continued. group versus NT control cells; ##*P*<0.01, ###*P*<0.001 for indicated comparisons. Ad-GFP indicates adenovirus encoding green fluorescent protein; AZ, azaserin; FCCP, Carbonyl cyanide 4-(trifluoromethoxy)phenylhydrazone; FK, FK866; HA, human influenza hemagglutinin tag sequence; NAD, nicotinamide adenine dinucleotide; NRC, neonatal rat cardiomyocyte; and NR, nicotinamide riboside.

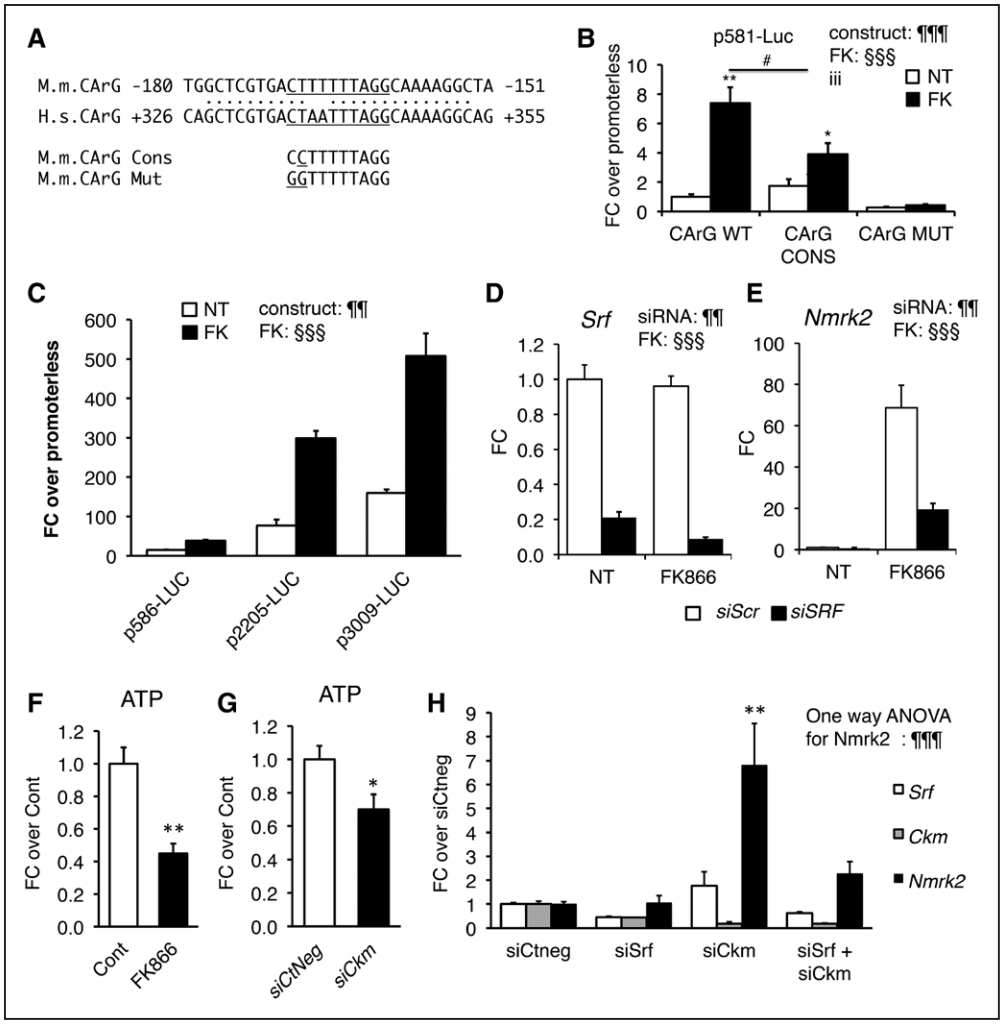

Figure 5. SRF is a component of *Nmrk2* gene transcription.
A, CArG-like binding site for SRF in the conserved region between the murine (M.m) *Nmrk2* promoter and human (H.s) *NMRK2* intron 1. The CArG-like motif was mutated to a CArG consensus sequence (cons) and a CArG mutant (mut) site unable to bind SRF. **B,** Activity of p586-Firefly Luciferase construct bearing wild-type (WT), consensus (CONS), or mutated (Mut) CArG motif without (NT) or with FK866 treatment (10 µmol/L) in NRC. SV40-renilla luciferase was cotransfected with the *Nmrk2*-Firefly Luc constructs for normalization of transfection efficiency. Two-way factorial ANOVA for independent factors: ¶¶¶P<0.001 for construct effect, §§§P<0.001 for FK effect; iii P≤0.001 for the interaction effect. Post hoc Tukey-test: *P<0.05, **P<0.01 FK versus NT; #P<0.05 CArG construct versus CArG wild type. **C**, Various lengths of the murine *Nmrk2* regulatory region were inserted into pGL4 vector and transfected in nontreated or FK866-treated NRC. Two-way factorial ANOVA for independent factors: ¶¶P<0.01 for construct effect, §§§P<0.001 for FK effect. **D** and **E,** *Srf* and *Nmrk2* mRNA levels in NRC transfected with control scrambled siRNA (siScr) (white bars), or *Srf* or *Nmrk2* siRNA (black bars), without (NT) or with FK866 treatment. Two-way factorial ANOVA for independent factors: ¶¶P<0.01 for siRNA effect, §§§P<0.001 for FK effect. **F** and **G,** ATP levels in NRCs treated for 72 hours with FK866 (**F**) or siCkm (**G**). *t* test: *P<0.05, **P<0.01, between FK-treated cells or siCkm-transfected cells versus control cells or siCtneg-transfected cells, respectively. **H,** *Srf*, *Ckm*, and *Nmrk2* mRNA level in NRC transfected for 72 hours with siRNAs as indicated. A 1-way ANOVA was used. ¶¶¶P≤0.001. Post hoc Tukey test: **P<0.01, between any group versus siCtneg-transfected control cells. Throughout the figure, data are expressed as mean±SEM over control group, fold change over control group (FC) except for **B** and **C**, fold change over promoterless pGL4 plasmid and **H** FC over siCtneg. CArG indicates $CC(A/T)_6GG$; NRC, neonatal rat cardiomyocyte; siRNA, small interfering RNA; and SRF, Serum Response Factor.

luciferase constructs into NRC and treated the cells with AICAR. The p586-Luc, and moreover, the p3009-Luc reporter, was highly responsive to AICAR treatment (Figure 6I and 6J). Cotransfection of a plasmid overexpressing a dominant negative isoform of AMPK efficiently blunted induction by AICAR (Figure 6I and 6J).

Analysis of the 5′-regulatory sequences of *Nmrk2* revealed enrichment in putative peroxisome proliferator–activated receptor (PPAR) binding sites (Figure 6K). The fragments –3009/–2552 and –1028/–228 contain most of the activity. By comparison, the activity of the *Nmrk2* promoter was very low in cardiac fibroblasts (Figure 6L).

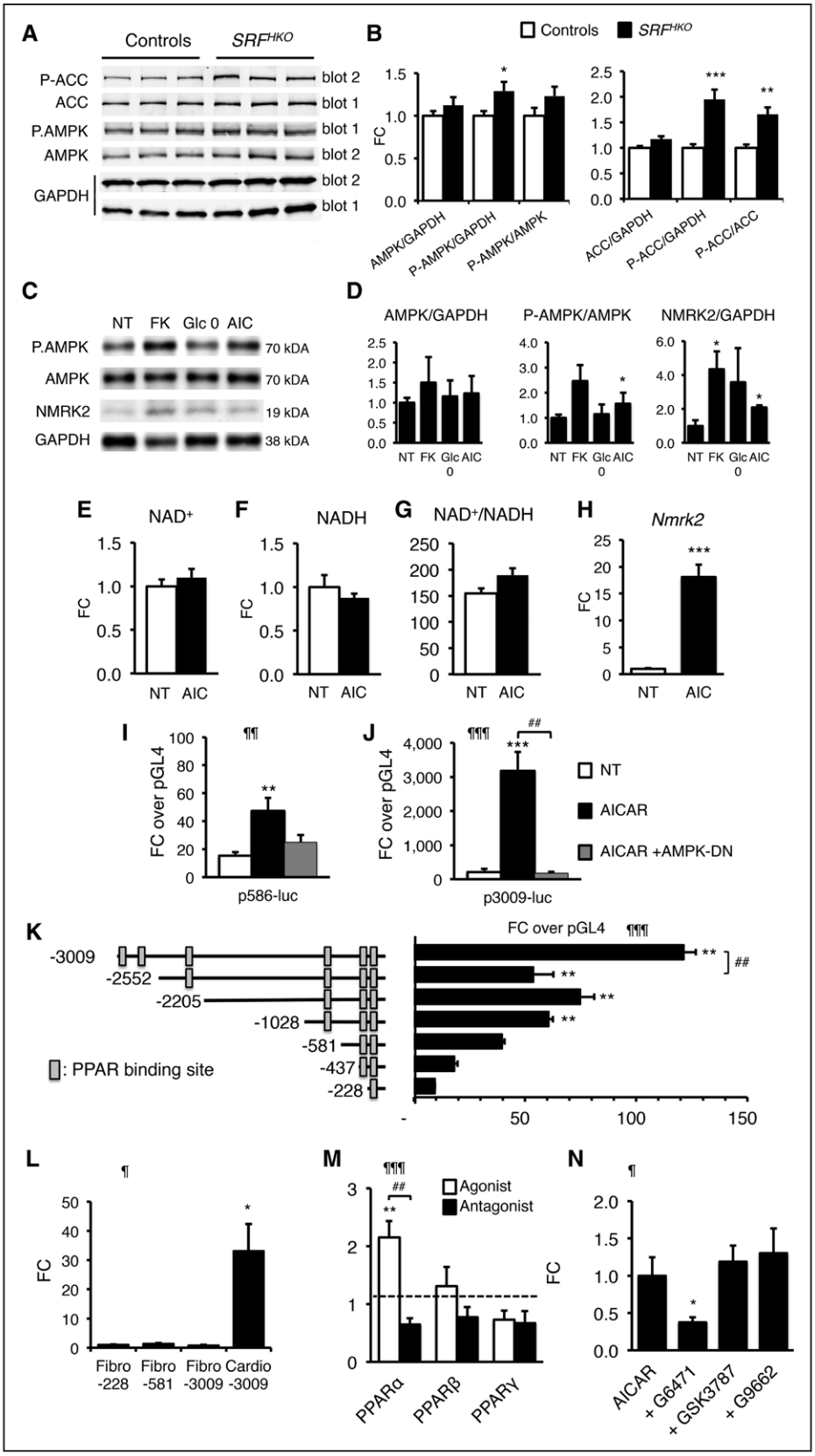

Figure 6. *Nmrk2* expression is increased by AMPK and PPARα pathways.
A, Representative Western blot analysis of cardiac proteins in control and *SRF*^{HKO} mice at day 9 using antibodies directed against ACC, phospho-ACC (Ser79), AMPKα, and phospho-AMPKα (Thr172). Phosphorylated and total proteins were analyzed on 2 separate gels (gel 1 and 2) and GAPDH antibody was used for loading control. **B,** Quantification (*Continued*)

To assess the role of PPAR factors in *Nmrk2* gene regulation, we cotransfected NRC with the p3009-Luc reporter and PPAR expression vectors. Only PPARα increased the activity of the *Nmrk2* promoter in the presence of its agonist GW7647 (Figure 6M). The PPARα antagonist G6471 repressed the *Nmrk2* promoter (Figure 6M) and blunted the activating effect of AICAR (Figure 6N). Neither the PPARβ nor the PPARγ antagonists had any effect on *Nmrk2* promoter induction by AICAR. These results establish that *Nmrk2* is an AMPK-PPARα–responsive gene that is induced by energy stress in cardiac cells.

NR Preserves Cardiac Function in the TAC Model

To determine whether NR treatment could be useful in other forms of HF, we assessed its efficiency in the TAC model of pressure overload cardiac hypertrophy. NR was administrated starting 2 days after the TAC or SHAM surgery. Kaplan-Meier survival curve analysis showed no significant difference, mainly because of a similar early mortality between the 2 groups within 1 week after TAC (Figure 7A). NR treatment reduced the final drop in LV ejection fraction that occurred between the fourth and sixth week after TAC (Figure 7B and Table V in the online-only Data Supplement). NR did not attenuate the dilatation of the LV chamber and had only a transient effect on the thinning of the interventricular septum (Figure 7C and 7D). At euthanization, the cardiac hypertrophy index was similar between the chow diet and NR groups (Figure 7E).

The TAC-induced HF resulted in a decrease of the myocardial NAD^+ pool, which was partially preserved by NR, with little impact on the NAD^+/NADH ratio (Figure 7F through 7H). TAC increased *Nmrk2* expression level in the nontreated group and NR-treated group, whereas *Nmrk1* expression remained unchanged and *Nampt* was repressed (Figure 7I through 7K). TAC repressed *Sirt3* expression, *Sirt1* and *Ckm* expression while increasing the expression of *Myh7*, *Anf*, and *Bnp* (Figure 7L through 7Q) but NR treatment had no impact on gene expression.

DISCUSSION

We report that depressed NAD^+ homeostasis and activation of NMRK2 kinase are early and persistent events in a mouse model of DCM leading to heart failure and that administration of NR, the substrate of NMRK2 and most energetically favorable NAD^+ precursor, prevents

Figure 6 Continued. of total and phosphoprotein signal from Western blot analyses. Data are normalized on GAPDH signal. The Phos/Total ratio is calculated from GAPDH normalized levels for each individual. n=6 for each group. Data are expressed as mean fold change (FC)±SEM over control group. *t* test: **P*≤0.05, ***P*≤0.01, ****P*≤0.001 over control group. **C,** NRCs were treated with FK866 (10 μmol/L, 72 hours, FK), AICAR (500 μmol/L, 48 hours, AIC), or grown in the absence of glucose in the medium (Glc 0) for 48 hours, and proteins were extracted for Western blot analyses. Representative Western blot. **D,** Quantification on n=3 samples for each condition of NRCs treated as in **C**. Data are expressed as mean FC±SEM over NT group. **P*≤0.05 over control group. **E** through **G,** Intracellular NAD^+ content (**E**), NADH (**F**), and NAD^+/NADH ratio (**G**) in NRCs after 24 hours of treatment with AICAR (500 μmol/L). **H,** RT qPCR analysis of *Nmrk2* mRNA level in NRCs treated with AICAR. *t* test: ****P*≤0.001 over nontreated control group. **I** and **J,** NRCs were cotransfected with *Nmrk2*-luciferase constructs containing 586 (**I**) or 3009 base pairs (**J**) of upstream *Nmrk2* regulatory region and a dominant negative (DN) AMPK expression vector. NRCs were transfected at day 3 after plating, followed by AICAR treatment (500 μmol/L) at day 4. Luciferase levels were analyzed at day 5. Normalized Fireflyl/Renilla values are expressed as in Figure 5B as FC±SEM over the promoterless pGL4 vector. One-way ANOVA: ¶¶*P*≤0.01, ¶¶¶*P*≤0.001 for treatment effect. Post hoc Tukey test: ***P*≤0.01, ****P*≤0.001 over nontreated control group. ##*P*<0.01 for AICAR versus AICAR+AMPK-DN. **K,** *Nmrk2* promoter deletion analysis by luciferase assay. Rectangular boxes show the position of the putative PPAR binding sites. Data are expressed as mean FC±SEM over the promoterless pGL4 plasmid. One-way ANOVA: ¶¶¶*P*≤0.001. Post hoc Tukey test: ***P*≤0.01, over the promoterless pGL4 vector. ##*P*<0.01 for over the immediately shorter construct. **L**, Neonatal rat cardiac fibroblasts and cardiomyocyte-enriched fractions were separated on a discontinuous Percoll gradient. Cardiac fibroblasts were transfected with the p-228, p-581, and p-3009-FLuc constructs. Cardiomyocytes were transfected with the p-3009-FLuc. SV40-RLuc construct was cotransfected for normalization. Data are expressed as mean FC±SEM over the mean p228-FLuc activity in cardiac fibroblasts. One-way ANOVA: ¶*P*≤0.05. Post hoc Tukey test: **P*≤0.05 Cardio-3009 over Fibro-30089. **M,** NRCs were cotransfected with the p3009-FLuc construct and the RXR expression vector and with either PPARα, PPAR β/δ, or PPARγ expression vectors. NRCs were treated 24 hours later with the agonists GW7647 (0.6 μmol/L), GW501516 (0.6 μmol/L), and G1929 (0.6 μmol/L), for PPARα, PPARβ/δ, and PPARγ, respectively, or with their respective antagonists, GW6471 (10 μmol/L), GSK3787 (2 μmol/L), or GW9662 (2 μmol/L). Data are expressed as mean FC±SEM over normalized luciferase levels of NRCs transfected with the p3009-FLuc construct alone (dashed line) in the same experiment. A 1-way ANOVA was used because each group is independent of the other (different agonists and antagonists): ¶¶¶*P*≤0.001. Post hoc Tukey test: ***P*≤0.01 versus p3009-FLuc alone. ##*P*≤0.01 for comparison between agonist and antagonist. **N,** NRCs were transfected with the p3009-FLuc construct. Transfected NRCs were treated 24 hours later with the antagonists G6471, GSK3787, or G9662, 30 minutes before adding AICAR for a further 24-hour period. All concentrations were as in **M**. Data are expressed as mean FC±SEM over the p3009-luc construct treated with AICAR alone. One-way ANOVA: ¶*P*≤0.05. Post hoc Tukey: **P*≤0.05 versus AICAR treated cells. ACC indicates acetyl-coenzyme A carboxylase; AICAR, 5-aminoimidazole-4-carboxamide ribonucleotide; AMPK, AMP-activated protein kinase; NRC, neonatal rat cardiomyocyte; NT, nontreated cells; PPAR, peroxisome proliferator-activated receptor; and RT qPCR, quantitative reverse transcription polymerase chain reaction.

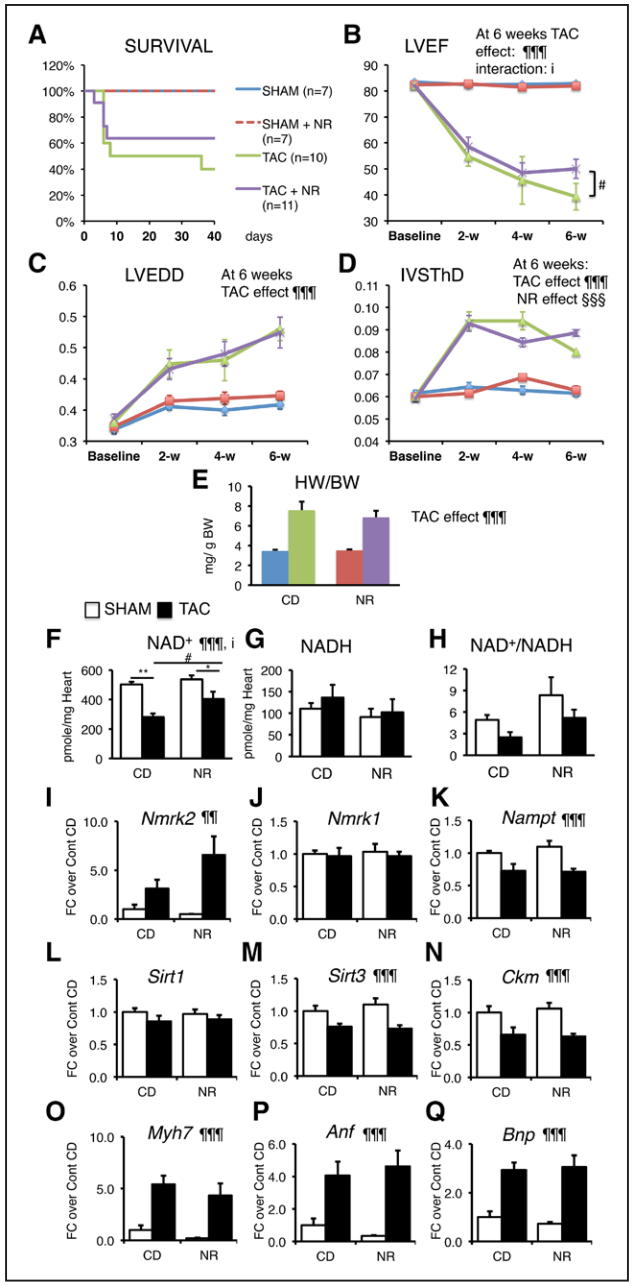

Figure 7. NR treatment preserves myocardial NAD levels and limits the drop in ejection fraction in the pressure overload–induced hypertrophy model. Two-month-old control and *SRF*^{HKO} male mice were subjected to TAC or SHAM surgery and fed with control chow diet (CD) or NR-enriched diet from day 2 after surgery to day 42. **A,** Kaplan-Meier survival curve analysis. Log-rank statistic: $P>0.05$. Color code shown on the right for each group is valid for **A** through **E**. **B** through **D,** Echocardiography follow-up analysis from baseline (2 days before surgery) to 6 weeks after. **E,** Heart weight to body weight ratio after euthanization at 6 weeks. **F** through **H,** Cardiac NAD$^+$ and NADH levels and redox state assessed by the NAD$^+$ cycling assay. **I** through **Q,** Cardiac mRNA levels of the indicated genes assessed by RT-qPCR. Data are expressed as mean±SEM. Statistical analysis: 2-way ANOVA for independent factors statistical analysis is shown at (*Continued*)

deterioration of cardiac function and adverse remodeling (Figure 8).

Altered NAD$^+$ homeostasis has been reported in several models of HF including pressure overload, myocardial infarction, and angiotensin 2 infusion.[3,37,38] In this context, much attention has focused on the NAMPT enzyme that is repressed in several models of cardiac injuries.[38] On the other hand, we found a robust upregulation of *Nmrk2* expression in the heart of *SRF*^{HKO} developing DCM and a more modest but significant increase following TAC-induced HF. It is interesting that we observed a similar shift from repressed NAMPT to increased NMRK2 in human failing heart. Interrogation of the Gene Expression Omnibus (GEO) database reveals that *Nmrk2* is induced in several models of cardiomyopathy related to mutations in the *lamin-A* (GEO data set GDS2746),[39] *Idh2* (GDS4893),[40] *PGC1α* (GDS4776),[41] or *Tfr1* (GSE68745)[42] genes. Considering the relative heterogeneity of molecular functions encoded by these genes, we propose that the activation of the NMRK2 pathway represents a common adaptive mechanism in the failing heart. Here, we show that the *Nmrk2* gene can be activated in response to NAMPT inhibition and activation of the energy stress sensor AMPK. In NRCs, we show that this activation depends on PPARα. PPARα is often expressed at lower levels in the adult failing heart,[43] whereas AMPK was shown to activate PPARα in various contexts.[44] Hence, AMPK activation could compensate in part for the lower levels of PPARα to activate *Nmrk2*. The precise contribution of these actors in the adult failing heart remains an open question. In the case of *SRF*^{HKO} hearts, it is interesting to note that, despite the fact that SRF is an upstream regulator of *Nrmk2* gene that we would expect to be repressed following *Srf* gene inactivation, SRF is also a major upstream regulator of *Ckm* gene, which is important to maintain PCr/ADP/ATP balance,[15,18] and AMPK is activated early on in the *SRF*^{HKO} heart (this study). We show in vitro that *Ckm* depression alone is sufficient to induce *Nmrk2* expression. In addition *Srf* inactivation alters the expression of numerous sarcomeric genes and triggers a severe eccentric remodeling[15] that is likely to further increase the energetic cost of contraction in vivo. A similar phenomenon could

Figure 7 Continued. 6 weeks and was used for **B** through **Q**, followed by post hoc Tukey test. ¶¶P≤0.01, ¶¶¶P≤0.001 for the TAC effect; §§§P≤0.001 for the NR treatment effect; i P≤0.05 for the interaction effect. Asterisks indicate statistically significant difference for the indicated comparisons: *P≤0.05, **P≤0.01. #P≤0.05 for the effect of NR within the TAC group. See accompanying Table V in the online-only Data Supplement for other echocardiography data at 6 weeks and previous stages. IVSThD indicates interventricular septum thickness in diastole; LVEDD, left ventricle end-diastolic diameter; LVEF, left ventricle ejection fraction; NAD, nicotinamide adenine dinucleotide; NR, nicotinamide riboside; RT-qPCR, quantitative reverse transcription polymerase chain reaction; and TAC, transverse aorta constriction.

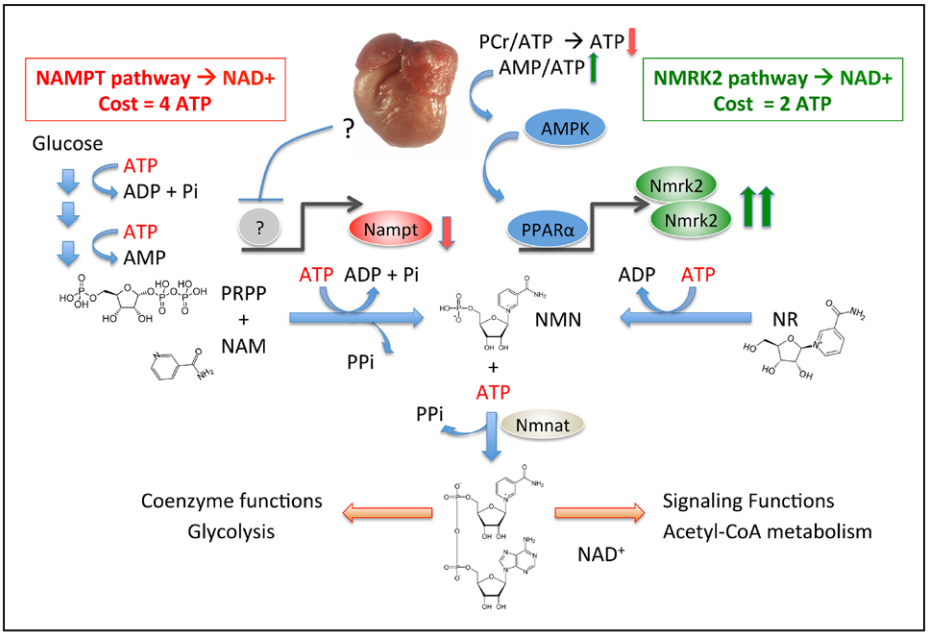

Figure 8. Activation of the NMRK2 pathway to NAD⁺ synthesis as an adaptive energy-sparing mechanism in the failing heart.

DCM is a form of pathological cardiac remodeling that is associated with severe energy depletion leading to HF. The energy stress sensor AMP-kinase is an adaptive signaling pathway aiming to preserve energy in the cells. The NAMPT enzyme is a major, rate-limiting step for NAD⁺ synthesis whose energetic cost equals 4 ATP molecules, including 1 converted to AMP, for the synthesis of 1 NAD⁺. NAMPT is repressed in most forms of HF through an unknown regulatory mechanism. Opposite to this repression, *Nmrk2* gene is an AMPK-responsive gene that is activated in several models of DCM and other forms of pathological remodeling such as the pressure-overload cardiac hypertrophy. NMR-kinase 2 allows the synthesis of NAD⁺ at a lower cost of 2 ATP per molecule. Although NR content may be limited in rodent and human diet, NR can easily be provided as a nutraceutical to help the failing heart to maintain NAD⁺ levels. AMPK indicates AMP-activated protein kinase; DCM, dilated cardiomyopathy; HF, heart failure; NAD, nicotinamide adenine dinucleotide; NAM, nicotinamide; NAMPT, nicotinamide phosphoribosyltransferase; NMN, nicotinamide mononucleotide; NR, nicotinamide riboside; PPAR, peroxisome proliferator-activated receptor; and PRPP, phosphoribosyl pyrophosphate.

occur for instance in the lamin-A mutants, which display severe alterations in cardiomyocyte cytoskeletal integrity and in which SRF activity is repressed and *Nmrk2* expression induced.[22,39] In addition to its well-known roles in stimulating fuel oxidation to restore ATP levels, we show that AMPK stimulation induces *Nmrk2* expression. NMN synthesis from NR by NMRK enzymes requires a single ATP, whereas synthesis from NAM by NAMPT requires >3 ATP equivalents: one for the autophosphorylation of the enzyme, and 2 (plus a carbohydrate) in formation of phosphoribosyl pyrophosphate (Figure 8). Both pathways consume an additional ATP for fusion with NMN to generate the dinucleotide. Hence, the shift from NAMPT to NMRK2 for NAD⁺ synthesis is an energy-sparing mechanism that may be favored in HF. In turn, we show that one of the beneficial actions of NR, at least in vitro, may be to increase glycolysis in cardiomyocytes. These different mechanisms of action may contribute to increase cardiac efficiency, which should be assessed in future studies to establish whether metabolic substrate preference and potentially glucose oxidation, which is associated with a better respiratory quotient and ATP availability, are improved on NR treatment.

Although the NMRK2 pathway is activated in the failing heart of SRF^{HKO} mice, the myocardial NAD⁺ level is depressed, which suggests that circulating and tissue levels of NAD⁺ precursors are insufficient to sustain cardiac NAD⁺ synthesis in mice on a regular rodent diet, stimulating an interest in NR supplementation to correct this defect. A few studies have shown that short-term NAD⁺ supplementation following chronic angiotensin-2 administration[37] or NMN supplementation following ischemia-reperfusion injury[45] or TAC surgery[46] can normalize alterations in NAD⁺/NADH ratio in the mouse failing heart. It is interesting to note that cells do not take up NMN intact, and, instead, NMN is extracellularly dephosphorylated to NR, such that its cellular conversion to NAD⁺ depends on the NR kinase pathway.[47,48]

We discovered a strongly beneficial effect of NR in the SRF^{HKO} model of HF in the preservation of cardiac function and limitation of cardiac remodeling that was associated with the maintenance of NAD⁺ levels in the heart. NAD⁺ metabolomics and expression analysis showed no evidence for increased levels of PAR, ADPR, Nam, or PARylated proteins, which would indicate a storm of NAD⁺-consuming activities in this model of

HF. Instead, a progressive loss of *Nampt* expression, coupled with the known depression of ATP and high-energy phosphates, is postulated to make it challenging for damaged hearts to maintain NAD^+ homeostasis.

Beyond the repletion in myocardial NAD^+ levels, the most striking NR-reversible deficit we found in HF was depression of CS and ACL activity. Many regulatory processes from gene expression to enzyme activity are controlled by reversible protein Lys acetylation. Although there is a variety of acetylases and deacetylases that are NAD^+-dependent and NAD^+-independent, production of citrate in mitochondria and its conversion to cytosolic Ac-CoA by the ACL is required to drive changes in substrate fuel selection[2] and protein acetylation level.[8,49] NR had no impact on the acetylation level of a mitochondrial protein like Aco2 but robustly increased the acetylation level of FOXO1 or p53 transcription factors in SRF^{HKO} hearts and control hearts, suggesting a tight link between NR-derived NAD^+ synthesis and Ac-CoA availability for posttranslational acetylation of nucleocytosolic proteins. This apparently overrides the ability of SIRT1 to deacetylate these factors. At the present stage, it is difficult to assess the consequences of these modifications. Moreover, there is presently no reason to think that FOXO1 and p53 are the only targets whose acetylation level is modified by long-term NR treatment. Rather, our data suggest that the acetylation levels of FOXO1 and p53 can be considered as surrogate markers of an increase in nucleocytosolic Ac-CoA metabolism.

Last, we observed that NR led to heightened production of Me4PY, a terminal NAM metabolite associated with local production of H_2O_2. This pathway was shown to promote life extension in the *Caenorhabditis elegans* through a hormetic response to a moderate rise in reactive oxygen species, which activates the cytoprotective NRF-2 transcription factor involved in oxidative stress response.[34] In the SRF^{HKO} heart, NR was shown to result in Me4PY simultaneous with induction of NRF-2.

Here, we also show a modest although significant protective effect of NR treatment on the drop of LV ejection fraction observed in the TAC model. The effect of NR in the TAC model seems to be less important than in the DCM model, which may be linked to the different nature of the cardiac stress in these models, ie, pressure overload in the TAC model that increases afterload versus volume overload in DCM that increases preload, and the fact that the *Nmrk2* gene is less strongly induced in the TAC model than in the SRF^{HKO} model. We note also that the early mortality induced by the TAC led to an early dropout in the untreated and NR-treated TAC groups that may have introduced a bias by removing from the analysis the animals with the worst outcome.

In conclusion, our work shows that oral NR supplementation is a powerful approach to preserve cardiac function and limit remodeling in DCM, a devastating disease currently lacking effective therapies. Recently, mutations in the de novo NAD^+ biosynthetic pathway were shown to lead to a new category of genetic diseases called congenital NAD deficiency disorders, which are associated with cardiac and skeletal defects but correctible by niacin supplementation in mouse models of the disease.[50] Our study and previous findings by others[13,26–28] suggest that NR has the potential not only to improve the cardiac symptoms in congenital syndromes and acquired HF, but also to act at a systemic level notably on liver metabolism, insulin resistance, and skeletal muscle performances that are altered concomitantly with cardiac defects. However, a limitation of our study is the fact that we did not study the impact of NR on the survival rate of SRF^{HKO} mice and the occurrence of terminal congestive HF. Further work will be required to determine the pharmacokinetics and pharmacodynamics of therapeutic NR administration in animal models and people with HF to enable safe and effective human translation.

ARTICLE INFORMATION

Received October 23, 2016; accepted November 6, 2017.

The online-only Data Supplement is available with this article at http://circ.ahajournals.org/lookup/suppl/doi:10.1161/CIRCULATIONAHA.116.026099/-/DC1.

Correspondence

Mathias Mericskay, PhD, Signalisation et Physiopathologie Cardiovasculaire, Inserm UMR-S 1180, Faculté de Pharmacie de l'Université Paris-Sud, 5, rue Jean-Baptiste Clément, F-92296 Chatenay-Malabry, France. E-mail mathias.mericskay@inserm.fr

Affiliations

Sorbonne Universités, Université Pierre et Marie Curie Paris 6, Department of Biology of Adaptation and Ageing, CNRS UMR8256, INSERM U1164, Institute of Biology Paris-Seine, DHU FAST, France (N.D., C.T., R.D., A. Gouge, J.B., J.-F.D., Z.L.). Department of Biochemistry, Carver College of Medicine, University of Iowa, Iowa City (S.A.J.T., C.B.). Signalling and Cardiovascular Pathophysiology, UMR-S 1180, University Paris-Sud, INSERM, Université Paris-Saclay, Châtenay-Malabry, France (C.T., R.D., J.P., M.G., B.M., M.B., A. Garnier, M.M.). Sorbonne Universités, Université Pierre et Marie Curie Paris 6, Plateforme PECMV, UMS28, Paris, France (N.M.). Institute of Metabolism and Systems Research, University of Birmingham, United Kingdom (G.G.L.). Department of Pharmacology and Pharmacotherapy, University of Szeged, Hungary (I.B.). Physiology Department, Faculty of Medicine and EA3072, Université de Strasbourg, France (J.Z.).

Acknowledgments

The authors thank V. Veksler and R. Ventura-Clapier (Inserm UMR-S 1180) for expert advice on respiration assays, Luc Bertrand (UCL, Belgium) for expert advice on AMPK detection, A. Angelini (UMR 8256) for technical help in these assays, A. Grosfeld (UMR 8256) for preliminary setup experiments for *Nmrk2* cloning, Florence Lefebvre for adult rat cardiomyocyte isolation.

Sources of Funding

This study was supported by the Association Française contre les Myopathies (AFM N 16282), the Agence Nationale de la Recherche (ANR) grant NAD-Heart ANR-17-CE17-0015-01 and ANR-08-GENOPAT-038, Fondation de France grant 00075811 and fundings from Institut National pour la Santé Et la Recherche Médicale (INSERM), Center National de la Recherche Scientifique (CNRS), Université Pierre et Marie Curie Paris 6, and University Paris Sud. Drs Diguet and Tannous, and Mr Deloux were supported by a PhD fellowship of French Ministère de

la Recherche et de l'Enseignement Supérieur. Dr Diguet was further supported by a 1-year PhD fellowship from AFM. Dr Brenner is supported by the Roy J. Carver Trust. GGL is supported by a Wellcome Trust Senior Fellowship (104612/Z/14/Z).

Disclosures

Dr Brenner has an intellectual property interest in uses of NR. He serves on the Scientific Advisory Board of ChromaDex, which distributes NR and is cofounder and the chief scientific advisor of Prohealthspan, which sells NR supplements. The other authors declare no competing financial interest.

REFERENCES

1. Ventura-Clapier R, Garnier A, Veksler V, Joubert F. Bioenergetics of the failing heart. *Biochim Biophys Acta*. 2011;1813:1360–1372. doi: 10.1016/j.bbamcr.2010.09.006.
2. Des Rosiers C, Labarthe F, Lloyd SG, Chatham JC. Cardiac anaplerosis in health and disease: food for thought. *Cardiovasc Res*. 2011;90:210–219. doi: 10.1093/cvr/cvr055.
3. Mericskay M. Nicotinamide adenine dinucleotide homeostasis and signalling in heart disease: Pathophysiological implications and therapeutic potential. *Arch Cardiovasc Dis*. 2016;109:207–215. doi: 10.1016/j.acvd.2015.10.004.
4. Lee CF, Tian R. Mitochondrion as a target for heart failure therapy: role of protein lysine acetylation. *Circ J*. 2015;79:1863–1870. doi: 10.1253/circj.CJ-15-0742.
5. Belenky P, Bogan KL, Brenner C. NAD+ metabolism in health and disease. *Trends Biochem Sci*. 2007;32:12–19. doi: 10.1016/j.tibs.2006.11.006.
6. Cantó C, Menzies KJ, Auwerx J. NAD(+) Metabolism and the control of energy homeostasis: a balancing act between mitochondria and the nucleus. *Cell Metab*. 2015;22:31–53. doi: 10.1016/j.cmet.2015.05.023.
7. Fouquerel E, Sobol RW. ARTD1 (PARP1) activation and NAD(+) in DNA repair and cell death. *DNA Repair (Amst)*. 2014;23:27–32. doi: 10.1016/j.dnarep.2014.09.004.
8. Ghanta S, Grossmann RE, Brenner C. Mitochondrial protein acetylation as a cell-intrinsic, evolutionary driver of fat storage: chemical and metabolic logic of acetyl-lysine modifications. *Crit Rev Biochem Mol Biol*. 2013;48:561–574. doi: 10.3109/10409238.2013.838204.
9. Bindu S, Pillai VB, Gupta MP. Role of sirtuins in regulating pathophysiology of the heart. *Trends Endocrinol Metab*. 2016;27:563–573. doi: 10.1016/j.tem.2016.04.015.
10. Oka S, Alcendor R, Zhai P, Park JY, Shao D, Cho J, Yamamoto T, Tian B, Sadoshima J. PPARα-Sirt1 complex mediates cardiac hypertrophy and failure through suppression of the ERR transcriptional pathway. *Cell Metab*. 2011;14:598–611. doi: 10.1016/j.cmet.2011.10.001.
11. Pillai JB, Isbatan A, Imai S, Gupta MP. Poly(ADP-ribose) polymerase-1-dependent cardiac myocyte cell death during heart failure is mediated by NAD+ depletion and reduced Sir2alpha deacetylase activity. *J Biol Chem*. 2005;280:43121–43130. doi: 10.1074/jbc.M506162200.
12. Bogan KL, Brenner C. Nicotinic acid, nicotinamide, and nicotinamide riboside: a molecular evaluation of NAD+ precursor vitamins in human nutrition. *Annu Rev Nutr*. 2008;28:115–130. doi: 10.1146/annurev.nutr.28.061807.155443.
13. Trammell SA, Weidemann BJ, Chadda A, Yorek MS, Holmes A, Coppey LJ, Obrosov A, Kardon RH, Yorek MA, Brenner C. nicotinamide riboside opposes type 2 diabetes and neuropathy in mice. *Sci Rep*. 2016;6:26933. doi: 10.1038/srep26933.
14. Lund LH, Edwards LB, Kucheryavaya AY, Benden C, Dipchand AI, Goldfarb S, Levvey BJ, Meiser B, Rossano JW, Yusen RD, Stehlik J. The Registry of the International Society for Heart and Lung Transplantation: Thirty-second Official Adult Heart Transplantation Report–2015; focus theme: early graft failure. *J Heart Lung Transplant*. 2015;34:1244–1254. doi: 10.1016/j.healun.2015.08.003.
15. Parlakian A, Charvet C, Escoubet B, Mericskay M, Molkentin JD, Gary-Bobo G, De Windt LJ, Ludosky MA, Paulin D, Daegelen D, Tuil D, Li Z. Temporally controlled onset of dilated cardiomyopathy through disruption of the SRF gene in adult heart. *Circulation*. 2005;112:2930–2939. doi: 10.1161/CIRCULATIONAHA.105.533778.
16. Tritsch E, Mallat Y, Lefebvre F, Diguet N, Escoubet B, Blanc J, De Windt LJ, Catalucci D, Vandecasteele G, Li Z, Mericskay M. An SRF/miR-1 axis regulates NCX1 and annexin A5 protein levels in the normal and failing heart. *Cardiovasc Res*. 2013;98:372–380. doi: 10.1093/cvr/cvt042.
17. Touvron M, Escoubet B, Mericskay M, Angelini A, Lamotte L, Santini MP, Rosenthal N, Daegelen D, Tuil D, Decaux JF. Locally expressed IGF1 propeptide improves mouse heart function in induced dilated cardiomyopathy by blocking myocardial fibrosis and SRF-dependent CTGF induction. *Dis Model Mech*. 2012;5:481–491. doi: 10.1242/dmm.009456.
18. Diguet N, Mallat Y, Ladouce R, Clodic G, Prola A, Tritsch E, Blanc J, Larcher JC, Delcayre C, Samuel JL, Friguet B, Bolbach G, Li Z, Mericskay M. Muscle creatine kinase deficiency triggers both actin depolymerization and desmin disorganization by advanced glycation end products in dilated cardiomyopathy. *J Biol Chem*. 2011;286:35007–35019. doi: 10.1074/jbc.M111.252395.
19. Chang J, Wei L, Otani T, Youker KA, Entman ML, Schwartz RJ. Inhibitory cardiac transcription factor, SRF-N, is generated by caspase 3 cleavage in human heart failure and attenuated by ventricular unloading. *Circulation*. 2003;108:407–413. doi: 10.1161/01.CIR.0000084502.02147.83.
20. Kuwahara K, Teg Pipes GC, McAnally J, Richardson JA, Hill JA, Bassel-Duby R, Olson EN. Modulation of adverse cardiac remodeling by STARS, a mediator of MEF2 signaling and SRF activity. *J Clin Invest*. 2007;117:1324–1334. doi: 10.1172/JCI31240.
21. Frank D, Rangrez AY, Poyanmehr R, Seeger TS, Kuhn C, Eden M, Stiebeling K, Bernt A, Grund C, Franke WW, Frey N. Mice with cardiac-restricted overexpression of Myozap are sensitized to biomechanical stress and develop a protein-aggregate-associated cardiomyopathy. *J Mol Cell Cardiol*. 2014;72:196–207. doi: 10.1016/j.yjmcc.2014.03.016.
22. Ho CY, Jaalouk DE, Vartiainen MK, Lammerding J. Lamin A/C and emerin regulate MKL1-SRF activity by modulating actin dynamics. *Nature*. 2013;497:507–511. doi: 10.1038/nature12105.
23. Bieganowski P, Brenner C. Discoveries of nicotinamide riboside as a nutrient and conserved NRK genes establish a Preiss-Handler independent route to NAD+ in fungi and humans. *Cell*. 2004;117:495–502.
24. Belenky P, Racette FG, Bogan KL, McClure JM, Smith JS, Brenner C. Nicotinamide riboside promotes Sir2 silencing and extends lifespan via Nrk and Urh1/Pnp1/Meu1 pathways to NAD+. *Cell*. 2007;129:473–484. doi: 10.1016/j.cell.2007.03.024.
25. Mouchiroud L, Houtkooper RH, Moullan N, Katsyuba E, Ryu D, Cantó C, Mottis A, Jo YS, Viswanathan M, Schoonjans K, Guarente L, Auwerx J. The NAD(+)/sirtuin pathway modulates longevity through activation of mitochondrial UPR and FOXO signaling. *Cell*. 2013;154:430–441. doi: 10.1016/j.cell.2013.06.016.
26. Cantó C, Houtkooper RH, Pirinen E, Youn DY, Oosterveer MH, Cen Y, Fernandez-Marcos PJ, Yamamoto H, Andreux PA, Cettour-Rose P, Gademann K, Rinsch C, Schoonjans K, Sauve AA, Auwerx J. The NAD(+) precursor nicotinamide riboside enhances oxidative metabolism and protects against high-fat diet-induced obesity. *Cell Metab*. 2012;15:838–847. doi: 10.1016/j.cmet.2012.04.022.
27. Cerutti R, Pirinen E, Lamperti C, Marchet S, Sauve AA, Li W, Leoni V, Schon EA, Dantzer F, Auwerx J, Viscomi C, Zeviani M. NAD(+)-dependent activation of Sirt1 corrects the phenotype in a mouse model of mitochondrial disease. *Cell Metab*. 2014;19:1042–1049. doi: 10.1016/j.cmet.2014.04.001.
28. Khan NA, Auranen M, Paetau I, Pirinen E, Euro L, Forsström S, Pasila L, Velagapudi V, Carroll CJ, Auwerx J, Suomalainen A. Effective treatment of mitochondrial myopathy by nicotinamide riboside, a vitamin B3. *EMBO Mol Med*. 2014;6:721–731. doi: 10.1002/emmm.201403943.
29. Trammell SA, Schmidt MS, Weidemann BJ, Redpath P, Jaksch F, Dellinger RW, Li Z, Abel ED, Migaud ME, Brenner C. Nicotinamide riboside is uniquely and orally bioavailable in mice and humans. *Nature Commun*. 2016;7:12948. doi: 10.1038/ncomms12948.
30. Garnier A, Zoll J, Fortin D, N'Guessan B, Lefebvre F, Geny B, Mettauer B, Veksler V, Ventura-Clapier R. Control by circulating factors of mitochondrial function and transcription cascade in heart failure: a role for endothelin-1 and angiotensin II. *Circ Heart Fail*. 2009;2:342–350. doi: 10.1161/CIRCHEARTFAILURE.108.812099.
31. Grozio A, Sociali G, Sturla L, Caffa I, Soncini D, Salis A, Raffaelli N, De Flora A, Nencioni A, Bruzzone S. CD73 protein as a source of extracellular precursors for sustained NAD+ biosynthesis in FK866-treated tumor cells. *J Biol Chem*. 2013;288:25938–25949. doi: 10.1074/jbc.M113.470435.
32. Belenky P, Christensen KC, Gazzaniga F, Pletnev AA, Brenner C. Nicotinamide riboside and nicotinic acid riboside salvage in fungi and mammals. Quantitative basis for Urh1 and purine nucleoside phosphorylase function in NAD+ metabolism. *J Biol Chem*. 2009;284:158–164. doi: 10.1074/jbc.M807976200.
33. Trammell SA, Brenner C. Targeted, LCMS-based metabolomics for quantitative measurement of NAD(+) metabolites. *Comput Struct Biotechnol J*. 2013;4:e201301012. doi: 10.5936/csbj.201301012.
34. Schmeisser K, Mansfeld J, Kuhlow D, Weimer S, Priebe S, Heiland I, Birringer M, Groth M, Segref A, Kanfi Y, Price NL, Schmeisser S, Schuster S, Pfeiffer AF, Guthke R, Platzer M, Hoppe T, Cohen HY, Zarse K, Sinclair DA, Ristow M. Role of sirtuins in lifespan regulation is linked

to methylation of nicotinamide. *Nat Chem Biol*. 2013;9:693–700. doi: 10.1038/nchembio.1352.
35. Preiss J, Handler P. Biosynthesis of diphosphopyridine nucleotide. II. Enzymatic aspects. *J Biol Chem*. 1958;233:493–500.
36. Galli U, Travelli C, Massarotti A, Fakhfouri G, Rahimian R, Tron GC, Genazzani AA. Medicinal chemistry of nicotinamide phosphoribosyltransferase (NAMPT) inhibitors. *J Med Chem*. 2013;56:6279–6296. doi: 10.1021/jm4001049.
37. Pillai VB, Sundaresan NR, Kim G, Gupta M, Rajamohan SB, Pillai JB, Samant S, Ravindra PV, Isbatan A, Gupta MP. Exogenous NAD blocks cardiac hypertrophic response via activation of the SIRT3-LKB1-AMP-activated kinase pathway. *J Biol Chem*. 2010;285:3133–3144. doi: 10.1074/jbc.M109.077271.
38. Hsu CP, Yamamoto T, Oka S, Sadoshima J. The function of nicotinamide phosphoribosyltransferase in the heart. *DNA Repair (Amst)*. 2014;23:64–68. doi: 10.1016/j.dnarep.2014.08.005.
39. Muchir A, Pavlidis P, Decostre V, Herron AJ, Arimura T, Bonne G, Worman HJ. Activation of MAPK pathways links LMNA mutations to cardiomyopathy in Emery-Dreifuss muscular dystrophy. *J Clin Invest*. 2007;117:1282–1293. doi: 10.1172/JCI29042.
40. Akbay EA, Moslehi J, Christensen CL, Saha S, Tchaicha JH, Ramkissoon SH, Stewart KM, Carretero J, Kikuchi E, Zhang H, Cohoon TJ, Murray S, Liu W, Uno K, Fisch S, Jones K, Gurumurthy S, Gliser C, Choe S, Keenan M, Son J, Stanley I, Losman JA, Padera R, Bronson RT, Asara JM, Abdel-Wahab O, Amrein PC, Fathi AT, Danial NN, Kimmelman AC, Kung AL, Ligon KL, Yen KE, Kaelin WG Jr, Bardeesy N, Wong KK. D-2-hydroxyglutarate produced by mutant IDH2 causes cardiomyopathy and neurodegeneration in mice. *Genes Dev*. 2014;28:479–490. doi: 10.1101/gad.231233.113.
41. Martin OJ, Lai L, Soundarapandian MM, Leone TC, Zorzano A, Keller MP, Attie AD, Muoio DM, Kelly DP. A role for peroxisome proliferator-activated receptor γ coactivator-1 in the control of mitochondrial dynamics during postnatal cardiac growth. *Circ Res*. 2014;114:626–636. doi: 10.1161/CIRCRESAHA.114.302562.
42. Xu W, Barrientos T, Mao L, Rockman HA, Sauve AA, Andrews NC. Lethal Cardiomyopathy in mice lacking transferrin receptor in the heart. *Cell Rep*. 2015;13:533–545. doi: 10.1016/j.celrep.2015.09.023.
43. Vega RB, Kelly DP. Cardiac nuclear receptors: architects of mitochondrial structure and function. *J Clin Invest*. 2017;127:1155–1164. doi: 10.1172/JCI88888.
44. Pol CJ, Lieu M, Drosatos K. PPARs: protectors or opponents of myocardial function? *PPAR Res*. 2015;2015:835985. doi: 10.1155/2015/835985.
45. Yamamoto T, Byun J, Zhai P, Ikeda Y, Oka S, Sadoshima J. Nicotinamide mononucleotide, an intermediate of NAD+ synthesis, protects the heart from ischemia and reperfusion. *PLoS One*. 2014;9:e98972. doi: 10.1371/journal.pone.0098972.
46. Lee CF, Chavez JD, Garcia-Menendez L, Choi Y, Roe ND, Chiao YA, Edgar JS, Goo YA, Goodlett DR, Bruce JE, Tian R. Normalization of NAD+ redox balance as a therapy for heart failure. *Circulation*. 2016;134:883–894. doi: 10.1161/CIRCULATIONAHA.116.022495.
47. Ratajczak J, Joffraud M, Trammell SA, Ras R, Canela N, Boutant M, Kulkarni SS, Rodrigues M, Redpath P, Migaud ME, Auwerx J, Yanes O, Brenner C, Cantó C. NRK1 controls nicotinamide mononucleotide and nicotinamide riboside metabolism in mammalian cells. *Nat Commun*. 2016;7:13103. doi: 10.1038/ncomms13103.
48. Fletcher RS, Ratajczak J, Doig CL, Oakey LA, Callingham R, Da Silva Xavier G, Garten A, Elhassan YS, Redpath P, Migaud ME, Philp A, Brenner C, Canto C, Lavery GG. Nicotinamide riboside kinases display redundancy in mediating nicotinamide mononucleotide and nicotinamide riboside metabolism in skeletal muscle cells. *Mol Metab*. 2017;6:819–832. doi: 10.1016/j.molmet.2017.05.011.
49. Wellen KE, Hatzivassiliou G, Sachdeva UM, Bui TV, Cross JR, Thompson CB. ATP-citrate lyase links cellular metabolism to histone acetylation. *Science*. 2009;324:1076–1080. doi: 10.1126/science.1164097.
50. Shi H, Enriquez A, Rapadas M, Martin EMMA, Wang R, Moreau J, Lim CK, Szot JO, Ip E, Hughes JN, Sugimoto K, Humphreys DT, McInerney-Leo AM, Leo PJ, Maghzal GJ, Halliday J, Smith J, Colley A, Mark PR, Collins F, Sillence DO, Winlaw DS, Ho JWK, Guillemin GJ, Brown MA, Kikuchi K, Thomas PQ, Stocker R, Giannoulatou E, Chapman G, Duncan EL, Sparrow DB, Dunwoodie SL. NAD deficiency, congenital malformations, and niacin supplementation. *N Engl J Med*. 2017;377:544–552. doi: 10.1056/NEJMoa1616361.

Nicotinamide Riboside Preserves Cardiac Function in a Mouse Model of Dilated Cardiomyopathy

Nicolas Diguet, Samuel A.J. Trammell, Cynthia Tannous, Robin Deloux, Jérôme Piquereau, Nathalie Mougenot, Anne Gouge, Mélanie Gressette, Boris Manoury, Jocelyne Blanc, Marie Breton, Jean-François Decaux, Gareth G. Lavery, István Baczkó, Joffrey Zoll, Anne Garnier, Zhenlin Li, Charles Brenner and Mathias Mericskay

Circulation. 2018;137:2256-2273; originally published online December 7, 2017;
doi: 10.1161/CIRCULATIONAHA.116.026099
Circulation is published by the American Heart Association, 7272 Greenville Avenue, Dallas, TX 75231

Print ISSN: 0009-7322. Online ISSN: 1524-4539

Circulation

CORRECTION

Correction to: Nicotinamide Riboside Preserves Cardiac Function in a Mouse Model of Dilated Cardiomyopathy

In the article by Diguet et al, "Nicotinamide Riboside Preserves Cardiac Function in a Mouse Model of Dilated Cardiomyopathy," which published ahead of print December 7, 2017, and appears in this issue of the journal (*Circulation*. 2018;137:2256-2273. DOI: 10.1161/CIRCULATIONAHA.116.026099), the following corrections were made.

Figure 3S of the preprint online version contained a picture of an anti-aconitase 2 immunoblot (blot 2) that was performed after stripping of the acetyl-lysine antibody used to label immunoprecipitated aconitase 2 (blot1). As the efficiency of the stripping procedure could not be guaranteed, the picture of blot 2 has been removed. Instead, a picture of the input proteins used for immunoprecipitation that were run at the same time in a parallel gel is shown, as well as an immunoblot for GAPDH for loading control (previously Supp. Figure S6A). The picture of blot 1 has also been enlarged to show that a single acetylated protein migrating as the same size than aconitase 2 is present in this region of the gel. A picture of control IgG immunoprecipitation of cardiac proteins followed by anti-Acetyl-Lysine immnunoblot showing the absence of non specific acetylated band in this region of the gel is now shown in a new Figure VIA in the online-only Data Supplement.

http://circ.ahajournals.org

Diguet et al. Nicotinamide riboside preserves cardiac function in a mouse model of dilated cardiomyopathy

SUPPLEMENTAL MATERIAL

Supplemental Methods

Transgenic mice

All experiments with animals conformed to the Directive 2010/63/EU of the European Parliament and were approved by the ethics committee Charles Darvin #5 (agreement 00369.01). *SRF^{HKO}* mice bear the tamoxifen-inducible α*-MHC-MerCreMer* transgene and the *Srf* floxed allele (*Sf/Sf*) as described previously.[1] Tamoxifen (Sigma T5648) was administrated by i.p. injection at a dose of 0.7 mg diluted in 100 μl peanut oil at D0, D1 and D2 to *SRF^{HKO}* mice and *Sf/Sf* control littermates at 9 month of age. The sex ratio was balanced in each group.

For phenylephrine administration, the series of mice treated with PE, 80 mg/kg/day for 15 days with Alzet osmotic micropumps and the impact of the treatment on cardiac parameters have been published previously.[2] TAC surgery was performed under ketamine/xylazine anesthesia. Briefly the upper cartilage of the sternum was open on less that 0.3 cm to get access to the aortic cross without requirement for artificial ventilation of the mice. A 27-Gauge needle was plied along the aortic cross between the branching of the right brachio-cephalic artery and the left carotid artery and 2 tight knots with a 6.0 suture were made around the aortic cross and the needle. The needle was quickly removed to allow the blood to go through and the skin sutured with 4.0 silk. Mice were administrated buprenorphine for the first 24h and monitored daily by trained staff to detect signs of pains or issues with the suture. Animal showing signs of prostration, and/or infections and/or inability to feed by themselves were sacrificed for ethical reasons.

NR supplementation

The soft pellets were prepared every 5 days by mixing 1.65 g of NR into 500 g of powdered SAFE A04 diet and 235 ml of water to reach 2.24 mg of NR / g (wet weight). Control diet was prepared in the same way omitting NR. Mice had ad libitum access to food and water. Mice (average body weight 31.3 ± 0.82 g, no difference between groups) consumed an average of 6 g of soft food per day, reaching a minimal daily intake of 450 mg NR/kg. No difference in food intake was observed between *SRF^{HKO}* and control mice. For NAM and NR i.p. administration, mice were injected daily at a dose of 1 μmole/ g body weight with 300 mM NAM or NR solution in saline.

Microarray and RT-PCR analysis

To evaluate the effects of SRF deletion on gene expression, total RNA was purified from *SRF^{HKO}* and control *Srf$^{fl/fl}$* hearts with the RNeasy fibrous tissue kit (Qiagen). We examined the effects of SRF inactivation on gene expression at 8 days after TAM injection, an early stage when SRF is already strongly diminished but cardiac functions are not altered and at 25 days after TAM injection, an intermediate stage when the LVEF starts to decrease and LV chamber begin to dilate.1 In addition, we compared the effect of phenylephrine (PE), an alpha-adrenergic agonist known to trigger cardiac hypertrophy, administrated at 80 mg/kg/day with Alzet osmotic minipumps from day 5 to 15 after TAM injection to *SRF^{HKO}* and control *Srf$^{fl/fl}$* as previously described.

Microarray analysis for each genotype was performed with four samples, each being hybridized to one Affymetrix GeneChip MOE 430 2.0 array (Affymetrix, Santa Clara, CA) with a coverage of 45,000 transcripts, corresponding to over 30,000 mouse genes. All technical microarray procedures were carried out by PartnerChip (Evry, France) under Affymetrix guidelines. Briefly, 2 μg of total RNA sample was used to synthesize double stranded cDNA with the SuperScript II double-stranded cDNA synthesis kit (Invitrogen Life Technologies, Carlsbad, CA) according to the manufacturer's instructions. Labeled cRNA was synthesized using the Affymetrix IVT amplification and labeling kit. 20 μg of purified, fragmented labeled cRNA were hybridized with an array at 45°C for 16 h in an Affymetrix 640 hybridization oven. The posthybridization process was performed in an Affymetrix Fluidics Station 450 according to the manufacturer's instructions. All gene chips were scanned on an Affymetrix GeneChip 3000 scanner, and data were extracted from scanned images using AFX GCOS 1.4 software. Background intensities were adjusted and normalized using GCRMA method implemented in R (version 2.4.1).

RT-qPCR

cDNAs were reverse transcribed from RNA (1.5 μg) extracted in TRIzol (Thermofisher) from cell cultures and tissues using the Superscript II Reverse Transcriptase (Life Technologies). Quantitative PCR was carried out on a Light Cycler 480 (Roche Diagnostics) using Fast Start SYBR Green Master (Roche Diagnostics). Quantification of gene expression was calculated as $R=2^{\Delta Ct(Ref\ Cp - target\ Cp)}$, with Hprt used as a as reference. Primers were designed using the NCBI Primer-BLAST software. Primer sequences are available on request.

Western Blot Analysis

Proteins were homogenized in a lysis buffer (Tris-HCl pH7.5 50 mM, NP40 Igepal 1%, NaCl, 150 mM, EDTA 1mM, DTT 1mM, Glycerol 10%) in the presence of proteases. phosphatases and deacetylases inhibitors (PMSF 0.5 mM, NaF 50 mM, PPiNa 5 mM, Roche protease cocktail inhibitor 1/100, Santa Cruz deacetylase cocktail inhibitor 1/100). Equal amounts of proteins (10 to 20 μg) were separated on SDS-PAGE and transferred to nitrocellulose membranes. Proteins were detected by overnight incubation at 4°C with primary antibodies followed by IRDye 700 or IRDye800 fluorescent antibodies (Li-Cor Biosciences. 1/2500) and scanned on an Odyssey CLx Infrared Imaging System (Li-Cor Biosciences). Acetyl-CoA Carboxylase (ACC): Thermoscientific # MA5-15025; dilution 1/1000. ACC Phospho-Ser79: Thermoscientific # PA5-17725; dilution 1/1000. Acetylated-Lysine Mouse mAb (Ac-K-103) : Cell Signaling #9681 ; dilution 1/1000. AMPKα: Cell Signaling #2532; dilution 1/1000. AMPKα (Phospho-Thr172): Cell Signaling #2535; dilution 1/1000. FKHR (H-128)(FoxO1): Santa Cruz BT # sc-11350; dilution 1/1000. AcFKHR (D-19): Santa Cruz BT # sc-49437; dilution 1/200. Acetyl-Lysine: Cell Signaling #9441; dilution 1/1000. Citrate Synthase: Abcam. GAPDH: Sigma #G9545; dilution 1/3000. Aconitase 2: Kind gift of Anne Laure Bulteau (Bulteau et al. Biochemistry. 2003;42(50):14846-55); dilution 1/500. HA epitope: Sigma #H6908; dilution 1/500. NMRK2: generated by BioGenes (see below); dilution 1/500. PARP: Cell Signaling #9532; dilution 1/1000. PAR (Anti-Poly (ADP-Ribose): Pharmingen #551813 dilution 1/500. p53 (acetyl K386): Abcam #ab52172; 1/500. Anti-Visfatin antibody (NAMPT) : Abcam #ab24149 ; 1/500.

Generation of rabbit polyclonal antibody against NMRK2 protein
Polyclonal antibody was generated in rabbits, immunized with a peptide sequence specific to the NMRK2 protein, verified and affinity purified and tested by BioGenes GmbH (Berlin, Germany). SDS-PAGE analysis using the NMRK2 antibody on cardiac muscle lysates was performed on membranes blocked with 5% milk using a 1/500 dilution, with a rabbit HRP secondary that was used at a 1/25,000 dilution and developed using a chemoluminescence.

Immunofluorescent staining
Hearts were harvested after cervical dislocation and washed in cold PBS. Frozen hearts section (10 μ m) were fixed in 3.7% formaldehyde in PBS at room temperature (RT) for 10 minutes followed by permeabilization in PBS/Triton X100 (0.2%) for 10 minutes. Endogenous mouse immunoglobulins were blocked by 1h. RT. incubation with monovalent anti-mouse IgG Fab fragments (Jackson Immunoresearch) followed by saturation of non-specific binding sites with 2% BAS and 10% goat serum. Sections were incubated o/n at 4°C with mouse monoclonal [clone 5B4.7] (IgG1) to human MIBP (=NMRK2) at 1/100 dilution in saturation solution (LSBio, Seattle, USA and kind gift from Dr Chuanyue Wu, University of Pittsburgh, USA). The day after, sections were incubated with FITC-coupled anti-hVIN-1vinculin antibody (Sigma. 1/100) and Cy3-couple antimouse IgG1 (Jackson Immunoresearch. 1/400). Confocal images were acquired on a Leica SP5 microscope with identical gain and offset parameters for all samples.

Echocardiography
Echocardiography was performed on lightly anesthetized mice given isoflurane (induction with 1% isoflurane 100% O2 and maintained with 0.2 to 0.25% isoflurane 100% O2) to maintain high cardiac frequency. Non-invasive measurements of left ventricular dimensions were evaluated using Doppler echocardiography (Vivid 7 Dimension/Vivid7 PRO; GE Medical Systems) with a probe ultrasound frequency range of 9–14 MHz. The two-dimensionally guided time-motion recording mode (parasternal long-axis view) of the left ventricle (LV) provided the following measurements: diastolic and systolic septal (IVS) and posterior wall thicknesses (LVPW); internal end-diastolic (LVEDD) and end-systolic diameters (LVESD); and heart rate. Each set of measurements was obtained from the same cardiac cycle. At least 3 sets of measurements were obtained from 3 different cardiac cycles. LV fractional shortening (FS) was calculated using the formula: (LVEDD – LVESD)/LVEDD × 100. LV myocardial volume (LVV), LV end-diastolic volume (EDV), and end-systolic volume (ESV) were calculated using a half-ellipsoid model of the LV. From these volumes, LV ejection fraction (EF) was calculated using the formula: (EDV – ESV) / EDV × 100. H/R ratio was calculated by the formula (PWThd + IVSThd)/ LVEDd. A "blinded" echocardiographer, unaware of the genotype and the treatment, performed the examinations.

NAD extraction and quantification
Frozen tissue powder was resuspended in 75% ethanol, 25% HEPES 10 mM pH7.1, buffer (20 μ l/mg of tissue). Extracts were warmed 5 min at 80° C, then directly cold on ice and centrifuge 5 min at 16 000 g. Tissues extracts were normalized on the weight of tissue used for extraction. NAD was extremely stable in this buffer and resistant to heat degradation over 60 minutes. Using spiking concentrations of known amounts of NAD^+

and NADH (Sigma-Aldrich) in pure buffered ethanol solution followed by dilutions in acid (HCl 0.1M) or basic (NaOH 0.1M) buffer, heating at 60°C for 30 minutes and neutralization with TRIS buffer pH7.1, we found that NAD+ was extremely stable after heating in acid condition (>99% recovery) while NADH was completely destroyed (<1% recovery). Heating in NaOH buffer led to some destruction of both NAD+ and NADH and this protocol was discontinued. Hence, we selected the protocol of selective acid-heating destruction of NADH in the cardiac samples for the determination of free NAD+ versus free NADH concentrations in these extracts, the buffered ethanol extracts were diluted 1/10 in HCl 0.1M and heated 30 minutes at 60°C to destroy NADH and then neutralized with Tris buffer at pH 7.1 before measuring NAD+. After adjustment of dilution factors, NADH levels were calculated by subtracting the NAD+ concentration to the non-heated ethanolic extract values: NADH = NADt (non-heated) - NAD+(heated). Kinetics of the reaction (OD at 550nm, every 30 seconds for 40 minutes) was followed on a TECAN Infinite F500 microplate reader. NAD was quantified in duplicates for each sample by comparison to a range of standard NAD+ concentration using linear regression curve equation method between NAD+ standard concentrations and the slope of the reaction in OD units/sec. For cell cultures, the wells were washed twice with PBS and scraped on ice in buffered ethanol (100 μl/well in 12-well plates or 50 μl/well in 24-well plates). Extracts were diluted in water to a final volume of 25 μl to reach a concentration that within the titration curve. We added 100 μL of reaction buffer (600 mM ethanol, 0.5 mM 3-(4.5-dimethylthiazol-2-yl)-2.5-diphenyltetrazolium bromide (MTT), 2 mM phenazine ethosulfate (PES), 120 mM Bicine (pH7.8), yeast alcohol dehydrogenase (SIGMA A3263 > 300 u/mg) 0.05 mg/ml. Kinetics of the reaction (OD at 550nm, every 30 seconds for 40 minutes) was followed on a TECAN Infinite F500 microplate reader. NAD was quantified in duplicates for each sample by comparison to a range of standard NAD^+ concentration using linear regression curve equation method between NAD+ standard concentrations and the slope of the reaction in OD units/sec. NAD+/NADH was obtained by the formula ([NADt]-[NADH])/ [NADH]. Proteins could not be reliably quantified after extraction by boiling buffered ethanol method but cells layers were confluent in all conditions. Hence, in neonatal rat cardiomyocytes where the number of cells have changes over the culture period, data are given as fold change over mean control values (untreated group) at the time of extraction. In adult rat cardiomyocytes that do not proliferate, 20,000 cells were seeded per well in 24-well plates and an average cylinder volume of 20 μm diameter and 100 μm length was used to estimate the cellular volume and calculate the concentration.

Isolation and treatments of neonatal and adult rat cardiomyocytes (NRC, ARC)

NRC were isolated as described previously.[3] 1-day-old rat pups were killed by decapitation and the cardiac ventricles were harvested and minced into 1 to 2-mm wide cubes with scissors. After washing with Tyrode solution, heart fragments were subjected up to 10 rounds of digestion with 0.05 mg/ml of Liberase Blendzyme 4 (Roche Applied Science) in 10 ml oxygenated Tyrode solution under agitation at 37°C for 10 minutes. The supernatant of the first digestion was discarded and the following digestions were centrifuged and the cell pellet dissociated in 2 ml of DMEM, 10% FCS. The different fractions were pooled and centrifuged on a discontinuous Percoll gradient (bottom 58.5%. top 40.5%. 30 min. 3000 rpm) to enrich in cardiomyocytes at the interface between the 2 Percoll solutions. Non cardiac cells containing mainly fibroblasts were at the top of the tubes. Neonatal cardiomyocytes were seeded at a density 5 × 105

cells/well in 6-well plates coated with 10 μg/ml of laminin (BD Biosciences) in DMEM without pyruvate, with glucose 4.5g/l, 10% horse serum, 5% FCS and cultured at 37 °C in 1% CO2 atmosphere. To assay the impact on NAD+ and Nmrk2 expression, Azaserin and FK866 drugs were added in the culture medium at day 5 and renewed every day when the treatment was prolonged over several days. The same was done for NAD+, NR and AICAR (5-aminoimidazole-4-carboxamide-1- β -D-ribofuranoside). AICAR was administrated for 24h only. Doses are indicated in the legends. For treatment of transfected cells (see next section), AICAR, FK866 and PPAR agonists and antagonist were administrated 1 day after transfection. PPAR agonists: GW7647 for PPAR α, GW501516 for PPAR β / δ and GW1929 for PPAR γ ; PPAR antagonists: GW6471 PPAR α, GSK3787 for PPAR β / δ and GW9662 for PPAR γ were ordered from SIGMA ALDRICH CHIMIE, Saint Quentin Fallavier, France. Adult rat cardiomyocytes (ARC) were isolated as previously described.2 ARC were seeded at 20,000 cells/well in 24-well plates and treated 2 hours after Ca2+ introduction and plating with 10 μM FK866, 20 μM Azaserin or 1 mM NR for 65h before NAD extraction. In all conditions, they were still more than 60% of rod-shaped cardiomyocytes after 65 h cultures. The treatment did not induce changes in cell shape or cell numbers.

Seahorse analyses

NRC were seeded at 60 000 cells/well in 96-well Seahorse plates. At day 3 of culture, FK866 (10 μM) and/or a range NR doses was added to the medium. Analyses were performed at day 8 of culture. After equilibrating the cells for 1h at 37°C in the Seahorse test medium, the mitochondrial stress protocol included sequential injection of oligomycin (2 μM final) to inhibit ATP synthase, FCCP (1 μM final) as the uncoupling agent and a final injection of Amytal (1 mM final) and Antimycine A (0.5 μM final). For the glycolytic reserve assessment protocol, Cells were deprived of glucose in a non-buffered medium for one hour before the analysis. Glucose was injected first at 10 mM final to measure glycolysis. Glycolytic capacity was measures as the maximal ECAR value after oligomycin injection (2 μM final), effectively shutting down ATP production by oxidative phosphorylation. Glycolytic reserve is defined as the difference between basal glycolysis and glycolytic capacity. The final injection is 2-deoxy-glucose (2-DG) at 50 mM to inhibit glycolysis. All ECAR values are given after deduction of non-glycolytic ECAR measurement.

Cloning of mouse Nmrk2 promoter in luciferase reporter plasmid and transfection procedure

The transcription initiation site of mouse Nmrk2 promoter was determined by 5'RACE and was conform to the reported site in the Genebank (NM_027120.2). The promoter of the mouse Nmrk2 gene was cloned from C57Bl6/N genomic DNA by PCR with forward primer CCTATGAGGTGAGAGGATCTCTG (-3009/-2987) and reverse primer CTTGGGGACTGGAGGTGACTGGTC (+61/+38), and inserted into a pGL4.10[luc2] luciferase reporter plasmid (Promega prod no E6651). Subsequent deletions were performed by enzymatic digestion or primer mediated subcloning of the original fragment. 2.5 x 105 cardiomyocytes in 12-well plates were co-transfected at day 2 of culture with 1 μg of Nmrk2 pGL4.10[luc2] constructs and 100 ng of pGL4.73[hRluc/SV40] Vector (Promega prod no E6911) as an internal control of transfection efficiency using Lipofectamine 2000 (Lifetechnology) as indicated by the

supplier. In the case of AICAR treatment, Luciferase activity was analyzed 48h later with the Dual-Luciferase Assay System (Promega).

AMPK, PPAR, RXR Vectors

The pcDNA3 vectors harboring dominant negative AMPK, PPAR α, PPAR β and PPAR γ as well as RXR genes were kindly provided by Pr. M. Raymondjean and collaborator, Dr M. Foretz.[4-6] These vectors were co-transfected at a dose of 100 ng / well in 24-well plates with 500ng of Nmrk2 luciferase constructs.

Cloning of mouse Nmrk2 cDNA into recombinant adenovirus

The cDNA of Nmrk2 was cloned by PCR amplification from reversed transcribed cardiac mRNA into pcDNA3HA vector, introducing a MYPYDVPDYALMAMEARIR sequence (HA tag is underlined) at the N-terminus of Nmrk2 open reading frame that replaced the first methionine. The HA tagged Nmrk2 cDNA was then subcloned into the pShuttle2 vector before to be inserted in the Adeno-X viral DNA (Clontech lab. Adeno-X Expression System 1). Pac1 Linearized recombinant adenoviral DNA was transfected in HEK 293 cells followed by rounds of infection to collect the adenoviral particles. Adenoviral titer was determined by the cytopathic effect method. NRCs were infected at day 3 of culture with 100 particles/cell.

Mitochondrial (mtDNA) and nuclear (nDNA) DNA content

Total DNA was extracted from left ventricle. Briefly, tissue were minced in 500 μ l of buffer 1 (TrisHCl 10 mM, NaCl 10 mM, EDTA 25 mM, SDS 1%, proteinase K 0.4mg/ml, pH 7.5) with cleaned scissors and incubated overnight at 37° C. After addition of 50 μ l of saturated NaCl solution, the homogenates were centrifuged at 500 g for 15 minutes. Isopropanol (500 μ l) was added to supernatants which were then incubated 45 minutes at -20° C. After a centrifugation at 16000 g for 20 minutes, the pellets were kept, washed with ethanol 70%, resuspended in buffer 2 and finally warmed at 70°C. mtDNA content was measured by real-time qPCR using specific primers for a mitochondrial gene (Dloop, forward primer ATAGCCGTCAAGGCATGAAA, reverse primer GATTGGGTTTTGCGGACTAA) and a nuclear gene (B2M (beta-2-microgobulin), forward primer TGGTAAAGCAAAGAGGCCTAA, reverse primer AGAAGTAGCCACAGGGTTGG). The difference between the threshold cycle (Ct) of nuclear gene and mtDNA gene (Δ Ct) was used to assess the mtDNA/nDNA ratio, which was calculated using the following formula: 2($2\ \Delta$ Ct). For details see.[7]

Measure of O_2 consumption rate in permeabilized cardiac fibers

Mitochondrial respiration was studied in situ in saponin-permeabilized cardiac muscle fibres using a Clarke electrode as previously described.8 Oxygen consumption was measured after successive addition of pyruvate-malate (1-4 mM), ADP (0.1 mM), creatine (12 mM), ADP (2 mM), glutamate (10 mM), succinate (15 mM), and amytal (an inhibitor of complex I, 1 mM) to respiration solution (in mM: 2.77 CaK2EGTA, 7.23 K2EGTA [100 nM free Ca2+], 6.56 MgCl2 [1 mM free Mg2+], 20 taurine, 0.5 DTT, 50 K-methane sulfonate [160 mM ionic strength], 20 imidazole, pH 7.1) at 23°C. From this protocol, sensitivity of mitochondrial respiration to external ADP and creatine were determined (Km ADP and Km creatine) and acceptor control ratio (ACR) was calculated from basal mitochondrial respiration rate (in the presence of pyruvate/malate 1/4 mM,

without ADP) and oxygen consumption after addition of 2mM ADP. Rates of respiration are given in nmoles O2/min/mg dry weight.

Biochemical studies

Frozen tissue samples were weighed, homogenized (Bertin Precellys 24) in ice-cold buffer (50 mg/ml) containing HEPES 5 mM (pH 8.7), EGTA 1 mM, DTT 1 mM and 0.1% Triton X- 100. Citrate synthase (CS), complex I and cytochrome oxidase (COX), activities were determined in homogenized ventricles as previously described.[8] Activities of enzymes were determined by standard spectrophotometric assays. Briefly, for citrate synthase (CS), approximately 0.5 μ g of protein were added in 1 ml of Buffer M (Trizma 100 mM (pH8), 5,5'-dittiobis-(2-Nitrobenzenoic acid) 0.1 mM, Acetyl-CoA 0.3 mM, oxaloacetic acid 0.5mM) and the absorbance at 412 nm was measured during 3 min. Cytochrome oxidase (COX) activity was determined by the addition of approximately 0.25 μ g of protein in 1 ml of phosphate buffer (K2HPO4 50 mM (pH 7.4)) containing 50 μ M Cytochrome c (cytochrome c were previously reduced at 90% using sodium dithionite). Loss of reduced cytochrome c were followed by measuring the absorbance at 550 nm during 3 min using fully oxidized cytochrome c (by addition of potassium ferricyanure in excess) as a reference. For the determination of complex I activity, 25 μ g of protein and 100 μ M NADH were added to 1 ml of C1 Buffer (41.1 mM KH2PO4, K2HPO4 8.8 mM, Decyl-ubiquinone 100 μ M, BSA 3.75 mg/ml, pH 7.4). Measurements of the absorbance at 340 nm during 3 min in the presence and in the absence of 5 mM rotenone were used to calculate activity of this complex. CS, COX and complex I activities were respectively calculated using an extinction coefficient of 13600 M-1.cm-1, 18500 M-1.cm-1 and 6220 M-1.cm-1 and rates are given in international unit (IU)/g prot. ATP citrate lyase activity was quantified in 1 ml of assay buffer (100 mM Tris-HCl, pH 8.7, 20 mM Potassium citrate monobasic, 10 mMdithiothreitol, 10 mM MgCl2, 500 unit/ml of Malic Dehydrogenase from porcine heart #M1567 from SIGMA, 330 μ M Coenzyme A sodium salt hydrate, 5 mM ATP, 140 μ M NADH) by measurement of the absorbance at 340 nm during 3 min before and after the addition of 200 μ M SB 204990 inhibitor of ACL (TOCRIS, Cat. No. 4962). The difference between the slopes of the 2 measurements was used to calculate activity of ACL using an extinction coefficient for NADH of 6220 M-1.cm-1.

Liquid chromatography coupled to mass spectrometry (LCMS) analyses of NAD metabolome.

NAD-related metabolites were quantified as previously described with a Waters Acquity LC interfaced with a Waters TQD MS operated in positive ion multiple reaction monitoring mode.[9] Metabolites were extracted as follows: pieces of myocardial tissue (≈10 mg) were snap frozen and pulverized in liquid nitrogen. Metabolites were extracted in 10 volumes (μ l / mg of tissue powder) of buffered ethanol (75% ethanol/25% 10 mM HEPES, pH 7.1, v/v) preheated to 80 °C. Samples were shaken at 1000 rpm in an 80 °C block for three minutes. Soluble metabolites were separated from particulate by refrigerated microcentrifugation (10 min, 16kg). Extracts were dried via speed vacuum for three hours before to be processed for the LCMS analysis. This method does not effectively preserve reduced co-factors. Hence NADH and NADPH levels were not reported in this assay.

Vascular reactivity measurement

Mice were anesthetized by intraperitoneal injection of pentobarbital (150 mg/kg). Mesenteric bed was quickly isolated and placed in an ice-cold "Krebs" solution of following composition (in mmol/L): NaCl 119, KCl 4.7, CaCl2(H2O)2 2.5, MgSO4(H2O)7 1.2, KH2PO4 1.2, glucose 11, NaHCO3 25, bubbled with 95% O2 and 5% CO2 to maintain pH at 7.4. First order mesenteric arteries (inner diameter 100 – 300 μm) were carefully dissected, cleaned-off from fat tissue and cut into 1-2 mm segments. Each segment was mounted in the chamber of a small vessel myograph (620 M, Danish Myo Technology A/S, Aarhus, Denmark) using 25 μm tungsten wire, as described previously.[10] Chambers were filled with Krebs solution, bubbled with 95% O2 - 5% CO2 mixture and kept at 37°C. Data were digitized using a Powerlab 8/30 (AD Instruments, Paris, France) and acquired using the Labchart7 software (AD Instruments). Vessels underwent a normalization procedure which consisted in stretching the vessels stepwise to construct tension – circumference relationship. Rings were eventually set at an internal circumference corresponding to 90% of the circumference the vessel would have if submitted to a transmural pressure of 100 mmHg (13.3 kPa). After an equilibration period of 45-60 min, contractile responses of the vessels were evaluated by challenging them either with increasing extracellular [K+] (using modified Krebs solution containing various amount of KCl, with equimolar substitution of NaCl). Other vessels were treated with increasing concentrations of the thromboxane A2 mimetic U46619 (Interchim, Montluçon, France), added cumulatively. All vessels were then washed with Krebs solution and contracted again with U46619 (3.10-7 mol/L). Relaxant responses to cumulative concentrations of either carbachol (Cch, muscarinic receptor agonist, Sigma-Aldrich) or (2-(N,N-Diethylamino)-diazenolate-2-oxide diethylammonium salt (DEA-NO), a nitric oxide donor (Enzo Life Sciences, Villeurbanne, France) were then evaluated. Contractile responses were expressed in mN/mm or relative to response to a solution containing 120 mmol/L extracellular [K+]. Relaxant responses were expressed in %, relative to the starting contraction amplitude obtained with 3.10-7 mol/L U46619. Concentration-response curves were fitted with the Hill equation using Prism7 software (GraphPad software, Inc., La Jolla, CA, USA), allowing to determine EC50 (mol/L) and maximal effect (Emax) for each experiment. Because for some responses the curve fitting was not successful, corresponding experiments were excluded from the EC50 and Emax analysis. All data were expressed as mean ± SEM of N experiments, where "N" represents the number of animals. Statistical analysis was performed using Prism7. Mann-Whitney test was used to compare EC50 and Emax. Also concentration-response curves were compared using 2-way ANOVA.

Statistical Analyses

For in vivo experiments, animals were randomly assigned into different treatment groups. To assess significance, we performed Student's t test for independent samples when the experimental design compared only 2 groups, or One-Way ANOVA for multiple group comparisons, or Two Way ANOVA for independent factors when appropriate for the experimental design. Tukey tests were used for comparison of specific experimental groups when One-way ANOVA gave a p value < 0.05 or, in the case of Two Way ANOVA for interaction p value < 0.05. Values are expressed as mean ±SEM.

Supplemental References

1. Parlakian A, Charvet C, Escoubet B, Mericskay M, Molkentin JD, Gary-Bobo G, De Windt LJ, Ludosky MA, Paulin D, Daegelen D, Tuil D and Li Z. Temporally controlled onset of dilated cardiomyopathy through disruption of the SRF gene in adult heart. *Circulation*. 2005;112:2930-9.
2. Tritsch E, Mallat Y, Lefebvre F, Diguet N, Escoubet B, Blanc J, De Windt LJ, Catalucci D, Vandecasteele G, Li Z and Mericskay M. An SRF/miR-1 axis regulates NCX1 and annexin A5 protein levels in the normal and failing heart. *Cardiovascular research*. 2013;98:372-80.
3. Diguet N, Mallat Y, Ladouce R, Clodic G, Prola A, Tritsch E, Blanc J, Larcher JC, Delcayre C, Samuel JL, Friguet B, Bolbach G, Li Z and Mericskay M. Muscle creatine kinase deficiency triggers both actin depolymerization and desmin disorganization by advanced glycation end-products in dilated cardiomyopathy. *The Journal of biological chemistry*. 2011.
4. El Hadri K, Denoyelle C, Ravaux L, Viollet B, Foretz M, Friguet B, Rouis M and Raymondjean M. AMPK Signaling Involvement for the Repression of the IL-1beta-Induced Group IIA Secretory Phospholipase A2 Expression in VSMCs. *PloS one*. 2015;10:e0132498.
5. Ravaux L, Denoyelle C, Monne C, Limon I, Raymondjean M and El Hadri K. Inhibition of interleukin-1beta-induced group IIA secretory phospholipase A2 expression by peroxisome proliferator-activated receptors (PPARs) in rat vascular smooth muscle cells: cooperation between PPARbeta and the proto-oncogene BCL-6. *Mol Cell Biol*. 2007;27:8374-87.
6. Woods A, Dickerson K, Heath R, Hong SP, Momcilovic M, Johnstone SR, Carlson M and Carling D. Ca(2+)/calmodulin-dependent protein kinase kinase-beta acts upstream of AMP-activated protein kinase in mammalian cells. *Cell metabolism*. 2005;2:21-33.
7. Dimmock D, Tang LY, Schmitt ES and Wong LJ. Quantitative evaluation of the mitochondrial DNA depletion syndrome. *Clinical chemistry*. 2010;56:1119-27.
8. Kuznetsov AV, Veksler V, Gellerich FN, Saks V, Margreiter R and Kunz WS. Analysis of mitochondrial function in situ in permeabilized muscle fibers, tissues and cells. *Nat Protoc*. 2008;3:965-976.
9. Trammell SA and Brenner C. Targeted, LCMS-based Metabolomics for Quantitative Measurement of NAD(+) Metabolites. *Computational and structural biotechnology journal*. 2013;4:e201301012.
10. Mulvany MJ and Halpern W. Contractile properties of small arterial resistance vessels in spontaneously hypertensive and normotensive rats. *Circ Res*. 1977;41:19-26.

Table I. Patients' characteristics.

Patients	Pathology	Age	Sex	NYHA class	CHF duration	LVEF	BNP pg/ml	Treatments
1	Cad	49	M	4	90 Mo	15 %	320	Ramipril
2	Cad	63	M	3	4 Mo	30 %	157.8	Enalapril
3	Nocm	56	M	3	28 Mo	35 %	500	Ramipril, Carvedilol
4	Hdcm	48	F	4	29 Mo	23 %	1249	Perindopril, Carvedilol

Cad: coronary artery disease, Nocm: non-obstructive cardiomyopathy, Hdcm: hypertrophic dilated cardiomyopathy. LVEF: left ventricular ejection fraction.
Human cardiac tissue control samples (LV, mean age 51 years ± 4.5, S.D, not in the table) were obtained from general organ donors whose non-diseased hearts were explanted to obtain pulmonary and aortic valves.

Table II. Expression level of genes involved in NAD homeostasis

Probe Set ID	Gene Symbol	Gene Title	Mut D8	Mut D25	Mut D25 +PE	Cont D25 +PE
1452944_at	Afmid /// Syngr2	arylformamidase /// synaptogyrin 2	1.19	0.78	0.92	0.65
1447638_at	Afmid /// Syngr2	arylformamidase /// synaptogyrin 2	0.99	0.90	0.88	0.92
1428885_at	Afmid /// Syngr2	arylformamidase /// synaptogyrin 2	1.31	0.97	1.08	0.97
1431722_a_at	Afmid	arylformamidase	0.97	1.01	0.96	0.99
1432492_a_at	Haao	3-hydroxyanthranilate 3,4-dioxygenase	0.99	0.99	0.98	1.00
1420437_at	Ido1	indoleamine-pyrrole 2,3 dioxygenase 1	0.83	1.09	0.99	1.01
1425778_at	*Ido2*	indoleamine-pyrrole 2,3 dioxygenase 2	0.99	0.96	0.95	0.97
1418998_at	Kmo	kynurenine 3-monooxygenase (kynurenine 3-hydroxylase)	0.99	0.98	0.97	1.00
1430570_at	Kynu	kynureninase (L-kynurenine hydrolase)	1.00	0.94	0.93	0.96
1451903_at	Kynu	kynureninase (L-kynurenine hydrolase)	1.00	0.99	0.97	1.00
1430359_a_at	Nadsyn1	NAD synthetase 1	1.00	0.89	0.85	0.92
1417190_at	**Nampt**	nicotinamide phosphoribosyl transferase	1.02	1.10	0.87 ¶	1.35
1448607_at	Nampt	nicotinamide phosphoribosyl transferase	1.33	1.41	0.99	1.14
1454748_at	Naprt1	nicotinate phosphoribosyltransferase domain containing 1	0.64	0.86	0.86	1.06
1425773_s_at	Nmnat1	nicotinamide nucleotide adenylyltransferase 1	0.85	0.92	0.89	1.00
1429819_at	Nmnat1	nicotinamide nucleotide adenylyltransferase 1	0.96	1.05	1.05	1.05
1436155_at	Nmnat2	nicotinamide nucleotide adenylyltransferase 2	0.78	1.00	0.95	0.98
1424899_at	**Nmnat3**	nicotinamide nucleotide adenylyltransferase 3	1.11	0.79	**0.67**	0.73
1432342_at	Nmnat3	nicotinamide nucleotide adenylyltransferase 3	1.00	0.97	0.97	0.98
1443149_at	Nmnat3	Nicotinamide nucleotide adenylyltransferase 3 (Nmnat3). mRNA	0.99	0.98	0.97	1.00
1459128_at	Nmnat3	Nicotinamide nucleotide adenylyltransferase 3 (Nmnat3). mRNA	0.99	0.92	0.90	0.96
1432342_at	Nmnat3	nicotinamide nucleotide adenylyltransferase 3	1.00	0.97	0.97	0.98
1443149_at	Nmnat3	Nicotinamide nucleotide adenylyltransferase 3 (Nmnat3). mRNA	0.99	0.98	0.97	1.00
1459128_at	Nmnat3	Nicotinamide nucleotide adenylyltransferase 3 (Nmnat3). mRNA	0.99	0.92	0.90	0.96
1425646_at	Nmrk1	nicotinamide riboside kinase 1	0.98	0.90	0.91	1.01
1447503_at	Nmrk1	nicotinamide riboside kinase 1	1.00	0.99	0.92	0.98
1453898_at	**Nmrk2**	nicotinamide riboside kinase 2	**8.87**	**30.6**	**57.4** ¶	**4.15**
1422974_at	**Nt5e**	5' nucleotidase. ecto (CD73)	1.48	**2.80**	**4.22** ¶	1.21
1428547_at	**Nt5e**	5' nucleotidase. ecto (CD73)	1.06	**1.63**	**2.42**	0.94
1416530_a_at	**Pnp**	purine-nucleoside phosphorylase	0.76	0.83	**0.74**	0.92
1453299_a_at	Pnp	Similar to purine-nucleoside phosphorylase / LOC545044	0.96	0.84	0.68	0.88
1418836_at	Qprt	quinolinate phosphoribosyltransferase	1.00	0.99	0.99	1.00

1418837_at	Qprt	quinolinate phosphoribosyltransferase	1.00	0.99	0.98	1.00
1419093_at	Tdo2	tryptophan 2,3-dioxygenase	0.99	0.99	0.98	1.00
1449337_at	Tdo2	tryptophan 2,3-dioxygenase	0.99	0.99	0.98	1.00
1455770_at	Tdo2	Tryptophan 2,3-dioxygenase. mRNA (cDNA clone MGC:25811 IMAGE:4159877)	0.99	0.99	0.98	1.00

Control (Cont) and *SRF*^{HKO} mutant (Mut) mice were sacrificed at day (D) 8 or 25 after first day of tamoxifen injection. A group of control and a group of mutant mice were treated with phenylephrine (PE) from D10 to 25 before sacrifice. RNA was extracted and processed for Affymetrix Mouse 430.2 Expression array. Genes with a fold change expression < or > to 1.3 and a p value < 0.05 compared to non-treated time-matched control are highlighted in bold font, green for upregulated genes, red for down-regulated genes. ¶, genes differentially regulated between Mutant D25+PE and Control D25+PE.

Table III. Pharmacological parameters CE_{50} and E_{max} obtained by analysis of concentration-response curves of [K^+], thromboxane mimetic U46619 and NO donor DEA-NO in mesenteric artery rings isolated from NR-supplemented or control mice.

		[K^+]	U46619	carbachol	DEA-NO
Control	**N**	6	6	4[a]	5
	CE_{50}	24.7 ± 2.7 mmol/L	18 ± 8 nmol/L	1.7 ± 0.6 µmol/L	0.20 ± 0.14 µmol/L
	E_{max}	3.0 ± 0.3 mN/mm	116 ± 4 %	62 ± 8 %	77 ± 6 %
NR	**N**	5[a]	6	3[a]	5
	CE_{50}	31.2 ± 4.0 mmol/L	19 ± 8 nmol/L	0.5 ± 0.1 µmol/L	0.19 ± 0.10 µmol/L
	E_{max}	3.0 ± 0.3 mN/mm	121 ± 15 %	53 ± 6 %	81 ± 3 %

E_{max} for U46619 was expressed relative to the contraction amplitude obtained with solution containing 120 mmol/L [K^+]. E_{max} for carbachol and DEA-NO were expressed in %, relative to the starting contraction amplitude obtained with U46619 (100% corresponding to full relaxation). [a]: because for some responses the curve fitting was not successful, corresponding experiments were excluded from the EC_{50} and E_{max} analysis.

Table IV. LCMS analysis of hepatic NAD metabolome from control and SRF^{HKO} mutant mice fed with regular CD diet or NR-enriched diet.

Liver (pmol/mg)	Control (n = 4)	Control + NR (n = 5)	Mutant (n = 6)	Mutant + NR (n = 5)	Anova
NAD	1615 ± 432	1916 ± 636	1163 ± 40	4245 ± 1225	§
NADP	118 ± 27	105 ± 23	117 ± 6	159 ± 15	
NAAD	5.2 ± 1.7	7.5 ± 3.2	1.7 ± 0.4	52.5 ± 31.5	
NMN	6.7 ± 3.2	9.1 ± 3.6	2.5 ± 0.4	23 ± 8.1	§
ADPR	107 ± 21	129 ± 38	89 ± 13	347 ± 76 **	§§, i
Uridine	43 ± 7	53 ± 11	58 ± 5	26 ± 4 *	i
Cytidine	2.5 ± 0.7	2.6 ± 1	3 ± 0.4	1 ± 0.6	
Inosine	311 ± 81	344 ± 54	432 ± 54	489 ± 56	¶
IMP	196 ± 35	210 ± 37	311 ± 32	317 ± 43	¶¶
UMP	292 ± 44	222 ± 25	243 ± 21	223 ± 15	
CMP	20.2 ± 1.6	18.2 ± 3	21.3 ± 0.8	16.5 ± 1.4	
NR [a]	2.7 ± 0.9	2.1 ± 0.4	1 ± 0.5	3.3 ± 1.3	
Nam	479 ± 126	433 ± 86	355 ± 124	956 ± 215 *	i
MeNam	4.2 ± 0.6	23.1 ± 5.3	3 ± 0.7	26.8 ± 6.8	§§
Me-4PY [b]	2.4 ± 0.5	11.7 ± 2.8	1.3 ± 0.5	17.6 ± 3.2	§§

(a) n=3 for Mutant (b) n=4 for Mutant

Liver metabolite extraction was performed in the same mice than those analyzed for the cardiac metabolome in the Figure 3 of the main manuscript.
Statistics: 2-way ANOVA for independent samples followed by post-hoc Tukey test: Genotype effect is indicated by ¶ p≤0.05, ¶¶ p≤0.01; NR effect is indicated by § p≤0.05, §§ p≤0.01. Interaction effect is indicated by i p≤0.05. Where interaction was detected, post-hoc Tukey test was performed between individual groups: * p≤0.05 NR vs CD for the same genotype.

Table V. Echocardiography after TAC or SHAM surgery

	Baseline					2W				
	SHAM	SHAM + NR	TAC	TAC + NR	Anova	SHAM	SHAM + NR	TAC	TAC + NR	Anova
N	7	7	10	11		7	7	5	7	
IVSThD	0.6 ± 0.02	0.6 ± 0	0.6 ± 0.02	0.6 ± 0.02	ns	0.6 ± 0.02	0.6 ± 0.02	0.9 ± 0.04	0.9 ± 0.04	ns
LVEDD	3.2 ± 0.08	3.2 ± 0.1	3.3 ± 0.08	3.4 ± 0.07	ns	3.6 ± 0.06	3.6 ± 0.09	4.2 ± 0.22	4.2 ± 0.17	¶¶
PWThD	0.6 ± 0.02	0.6 ± 0.02	0.6 ± 0.04	0.6 ± 0.04	ns	0.6 ± 0.02	0.6 ± 0.04	0.7 ± 0.08	0.7 ± 0.03	¶¶
IVSThS	1 ± 0.03	1.1 ± 0.02	1 ± 0.03	1.1 ± 0.02	ns	1.1 ± 0.03	1.1 ± 0.03	1.2 ± 0.06	1.2 ± 0.06	¶¶
LVESD	1.7 ± 0.04	1.8 ± 0.06	1.8 ± 0.04	1.9 ± 0.04	ns	2 ± 0.04	2 ± 0.05	3.2 ± 0.26	3.1 ± 0.22	¶¶
PWThS	1.1 ± 0.05	1.1 ± 0.04	1.1 ± 0.04	1 ± 0.02	ns	1.1 ± 0.04	1 ± 0.02	0.9 ± 0.07	0.9 ± 0.03	¶¶
EDV	85 ± 5.7	87 ± 7.8	93 ± 6	98 ± 6	ns	115 ± 5.7	123 ± 9.2	192 ± 30.9	184 ± 20.5	¶¶
ESV	13 ± 1.8	14 ± 2	18 ± 2	17 ± 1.4	ns	20 ± 0	21 ± 1.4	90 ± 20	80 ± 15	¶¶
LVEF %	83 ± 0.4	82 ± 0.7	82 ± 0.3	82 ± 0.4	ns	82 ± 0.4	83 ± 0.3	55 ± 3.8	59± 3.7	¶¶
FS %	46± 0.5	45 ± 0.7	45 ± 0.3	47 ± 2.6	ns	45 ± 0.4	45 ± 0.32	24 ± 2.3	27± 2.3	¶¶
SV	71 ± 5.1	71 ± 7	75 ± 4.3	84 ± 4.9	ns	94 ± 4.8	103 ± 7.1	102 ± 10.2	106 ± 7.2	ns
h/r	0.4 ± 0.01	0.4 ± 0.01	0.4 ± 0.01	0.4 ± 0.01	ns	0.3 ± 0.01	0.3 ± 0.02	0.4 ± 0.03	0.4 ± 0.02	¶¶
HR	638 ± 9.7	605 ± 6.7	616 ± 8.4	614 ± 7.1	ns	638 ± 9.7	629 ± 12.8	549 ± 37.8	591 ± 12.3	¶¶
CO	46 ± 3.7	43 ± 4.4	46 ± 2.8	51 ± 2.9	ns	60 ± 3.3	65 ± 4.4	55 ± 2.3	62 ± 3.6	ns
LV mass	54 ± 1.8	55 ± 3.4	59 ± 5.2	58 ± 4.3	ns	66 ± 3.2	67 ± 5	136 ± 13.7	126 ± 9.8	¶¶
	4w					6w				
N	7	7	5	7	Anova	7	7	4	7	Anova
IVSThD	0.6 ± 0.02	0.7 ± 0.02	0.9 ± 0.04	0.8 ± 0.02 **, #	¶¶, ii	0.6 ± 0.02	0.6 ± 0.02	0.8 ± 0	0.9 ± 0.02	¶¶, §§
LVEDD	3.5 ± 0.09	3.7 ± 0.1	4.3 ± 0.33	4.4 ± 0.2	¶¶	3.6 ± 0.07	3.7 ± 0.08	4.8 ± 0.19	4.7 ± 0.25	¶¶
PWThD	0.5 ± 0.02	0.6 ± 0.03	0.8 ± 0.08	0.8 ± 0.07	¶¶	0.6 ± 0.04	0.6 ± 0.03	0.7 ± 0.06	0.8 ± 0.05	¶¶
IVSThS	1.1 ± 0.04	1.1 ± 0.03	1.2 ± 0.07	1 ± 0.02	i	1.1 ± 0.04	1.1 ± 0.02	1.1 ± 0.03	1.1 ± 0.05	ns
LVESD	1.9 ± 0.05	2.1 ± 0.06	3.5 ± 0.47	3.5 ± 0.23	¶¶	1.9 ± 0.04	2.1 ± 0.06	4.1 ± 0.26	3.7 ± 0.28	¶¶
PWThS	1 ± 0.04	1.1 ± 0.04	1.1 ± 0.07	1 ± 0.03	ns	1.1 ± 0.04	1 ± 0.04	0.8 ± 0.05	1 ± 0.05	¶¶
EDV	109± 7.4	129 ± 9.9	206 ± 42.5	217 ± 24.8	¶¶	119 ± 5.9	139 ± 6.7	272 ± 28.7	270 ± 35.4	¶¶
ESV	19 ± 1.4	23 ± 1.8	128 ± 39.2	116 ± 19.1	¶¶	19 ± 1.4	24 ± 2	167 ± 27.5	143 ± 25.9	¶¶
LVEF %	82 ± 0.5	81 ± 0.3	46 ± 9.1	48 ± 3.7	¶¶	83 ± 0.4	82 ± 0.5	39 ± 5.1**	50 ± 3.7 **, #	¶¶, i
FS %	45 ± 0.6	44 ± 0.3	20 ± 5.2	21 ± 2	¶¶	45 ± 0.5	45 ± 0.5	16 ± 2.6***	22 ± 2.1 **, ##	¶¶, i
SV	91 ± 6.3	104 ± 8.4	80 ± 4.5	100 ± 9	ns	97 ± 5.2	110 ± 4.4	105 ± 6.5	130 ± 11.3	¶¶
h/r	0.3 ± 0.01	0.4 ± 0.02	0.4 ± 0.04	0.4 ± 0.01	ns	0.3 ± 0.01	0.3 ± 0.01	0.3 ± 0.03	0.4 ± 0.02	¶¶
HR	645 ± 11	636 ± 10.8	575 ± 20.7	586 ± 20.9	¶¶	628 ± 6.5	636 ± 10.7	598 ± 38.7	568 ± 24.6	¶¶
CO	59 ± 4.7	67 ± 6	46 ± 1.6	62 ± 2.9	§	61 ± 3.3	70 ± 3.3	63 ± 6.2	74 ± 7.6	ns
LV mass	62 ± 3.6	80 ± 3.8	156 ± 22.6	141 ± 15.8	¶¶	65 ± 5.1	72 ± 4.2	146 ± 6.3	173 ± 18.3	¶¶

Abbreviations: IVSThD and IVSThD, interventricular septum thickness in diastole and systole; LVEDD and LVESD, left ventricle end-diastolic and end-systolic diameter; PWTh, LV posterior wall thickness; EDV and ESV, end-diastolic and end-systolic volume; LVEF, LV ejection fraction; FS, LV fractional shortening; h/r, LV wall thickness/radius ratio; HR, heart rate; CO, cardiac output. Two-way factorial ANOVA for independent samples: ¶¶ $p \leq 0.01$ for the TAC effect; § $p \leq 0.05$, §§ $p \leq 0.01$ for the NR effect; i $p < 0.05$, ii $p \leq 0.01$ for the interaction effect. ANOVA was followed by a post-hoc Tukey test when interaction was significant: **, $p \leq 0.01$, ***, $p \leq 0.001$ vs the SHAM group; #, $p \leq 0.05$, ##, $p \leq 0.01$ for the effect of NR within the TAC group.

Table VI: Antibody list

Target protein	**Antibody Supplier. ref #**	**Dilution**
Acetyl-CoA Carboxylase (ACC)	Thermoscientific. # MA5-15025	1/1000
ACC Phospho-Ser79	Thermoscientific. # PA5-17725	1/1000
AMPKα	Cell Signaling #2532	1/1000
AMPKα (Phospho-Thr172)	Cell Signaling #2535	1/1000
FKHR (H-128)(FoxO1)	Santa Cruz BT. # sc-11350	1/1000
Ac-FKHR (D-19):	Santa Cruz BT..# sc-49437	1/200
Acetyl-Lysine	Cell Signaling #9441	1/1000
Citrate Synthase	Abcam	
GAPDH	Sigma #G9545	1/3000
Aconitase 2	Kind gift of Anne Laure Bulteau (Bulteau et al. Biochemistry. 2003;42(50):14846-55)	1/500
HA epitope	Sigma #H6908	1/500
NMRK2	Generated by BioGenes (see below)	1/500
PARP	Cell Signaling #9532	1/1000
PAR (Anti-Poly (ADP-Ribose)	Pharmingen #551813	1/500
p53 (acetyl K386)	Abcam #ab52172	1/500

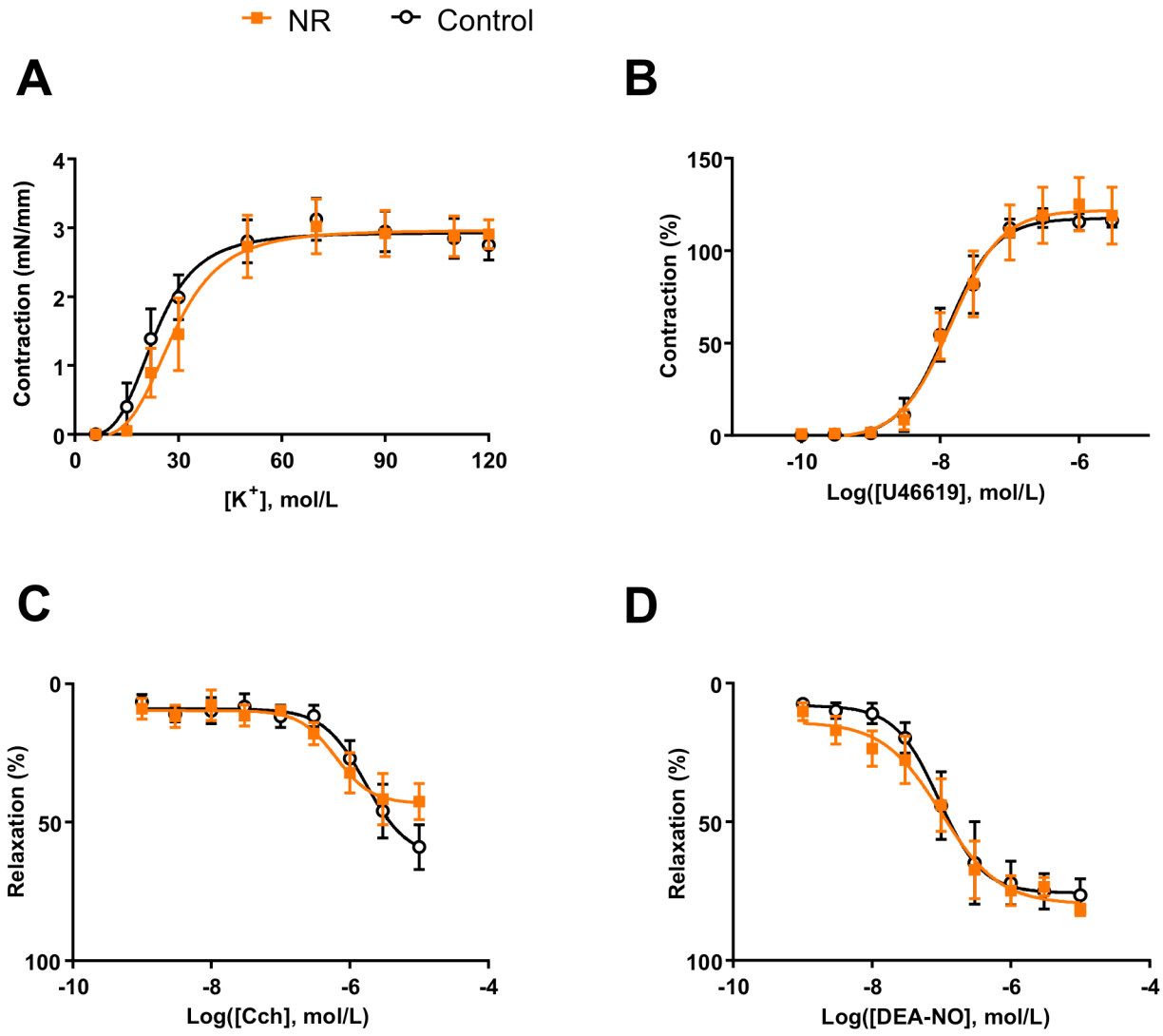

Figure I. NR supplementation did not alter vascular reactivity of isolated mesenteric artery rings. Vasomotor response curves to increasing concentrations of K^+ (A), the thromboxane mimetic U46619 (B), the muscarinic receptor agonist carbachol (Cch, C) or the NO donor diethylamine-nonoate (DEA-NO, D) were studied on mesenteric artery rings isolated from NR-supplemented mice (NR, filled squares) or control mice (Control, empty circles). In B, contraction was expressed relative to the contraction amplitude obtained with solution containing 120 mmol/L [K^+]. In C and D, relaxant responses were expressed in %, relative to the contraction amplitude obtained with U46619. Data are mean ± SEM of N=5-6 animals. No significant difference was found between NR and control groups in any of the response tested (2-way ANOVA).

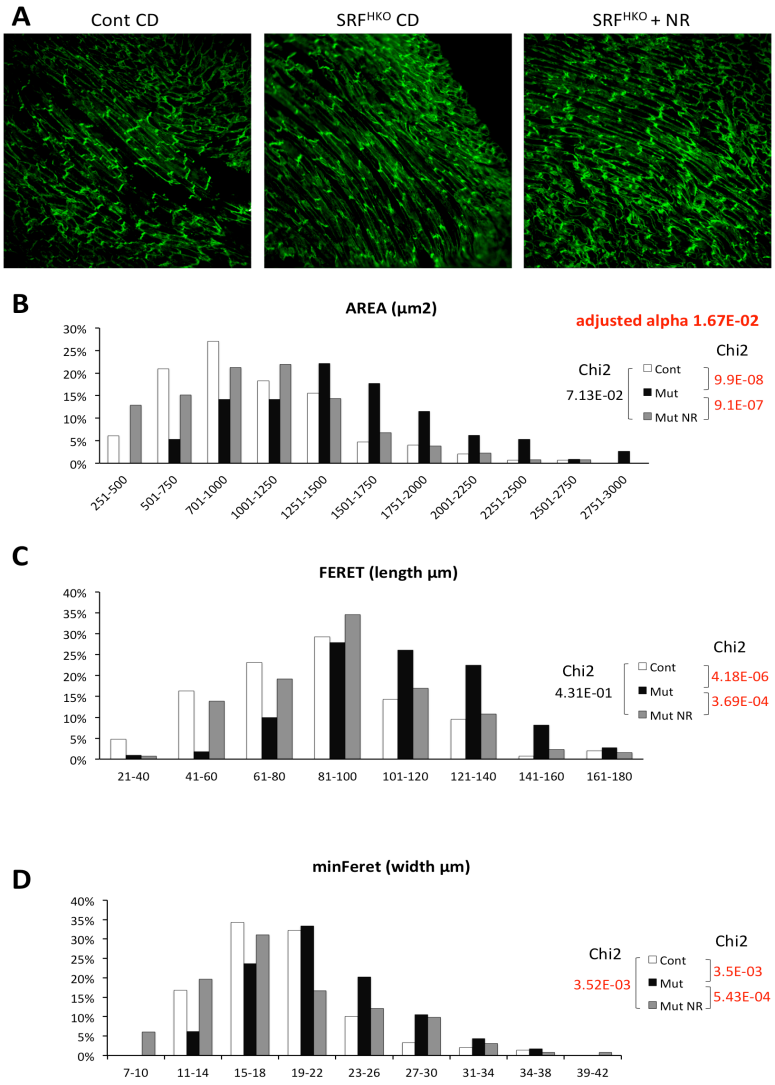

Figure II. Histological assessment of cardiomyocytes shape in SRF^{HKKO} mice fed with control diet or NR-enriched diet compared to control mice on regular control diet. (A) Transverse heart section taken in the middle region between apex and base were stained with Anti h1-Vinculin staining was used to label cardiomyocytes sarcolemma and intercalated disks. Confocal images were acquired in the middle of the posterior wall of the LV were cardiomyocytes are cut in the longitudinal axis. **(B)** Cardiomyocytes area, **(C)** length (Feret) and **(D)** width (minFeret) were calculated using Image J software in 3 independent mice for each group. Statistics: A Chi2 test was applied to test the frequency distribution of cardiomyocytes. Alpha level was adjusted to 1.67E-2 (0.05 / 3 comparisons). Control N=3, 148 cardiomyocytes; Mut SFR^{HKO} N=3 individual, 113 cardiomyocytes; Mut SRF^{HKO} + NR, N=3 individuals, 132 cardiomyocytes.

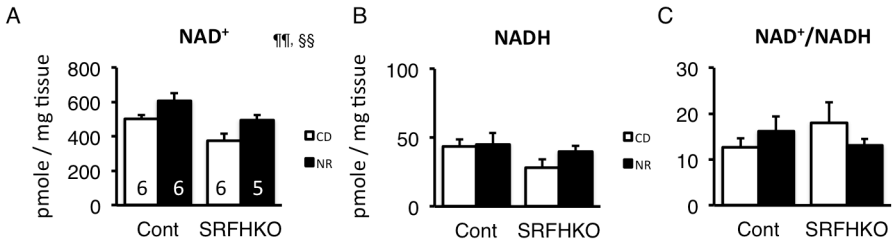

Figure III. Cardiac NAD⁺ and NADH quantification in control and SRF^{HKO} mice at day 50 following 45 days of NR enriched diet.

Cardiac metabolites were extracted by the boiling method in buffered ethanol. The extracts containing the sum of free NAD⁺ and NADH (total free NAD) or NAD⁺ only after selective heat degradation of NADH in acid conditions were quantified by the colorimetric alcohol dehydrogenase NAD recycling assay. NADH levels were calculated by the substraction of quantified NAD+ levels from total NAD. **(A)** NAD⁺ values in pmole/ mg of heart tissue; control CD n=6, control NR n=6, SRFHKO CD n=6, SRFHKO NR n=5. **(B)** NADH values in pmole/ mg of heart tissue, control CD n=5, control NR n=6, SRFHKO CD n=5, SRFHKO NR n=4. **(C)** NAD⁺/NADH ratio. Two-way factorial ANOVA for independent samples: ¶¶ p≤ 0.01 for the genotype effect; §§ p≤ 0.01 for the NR effect.

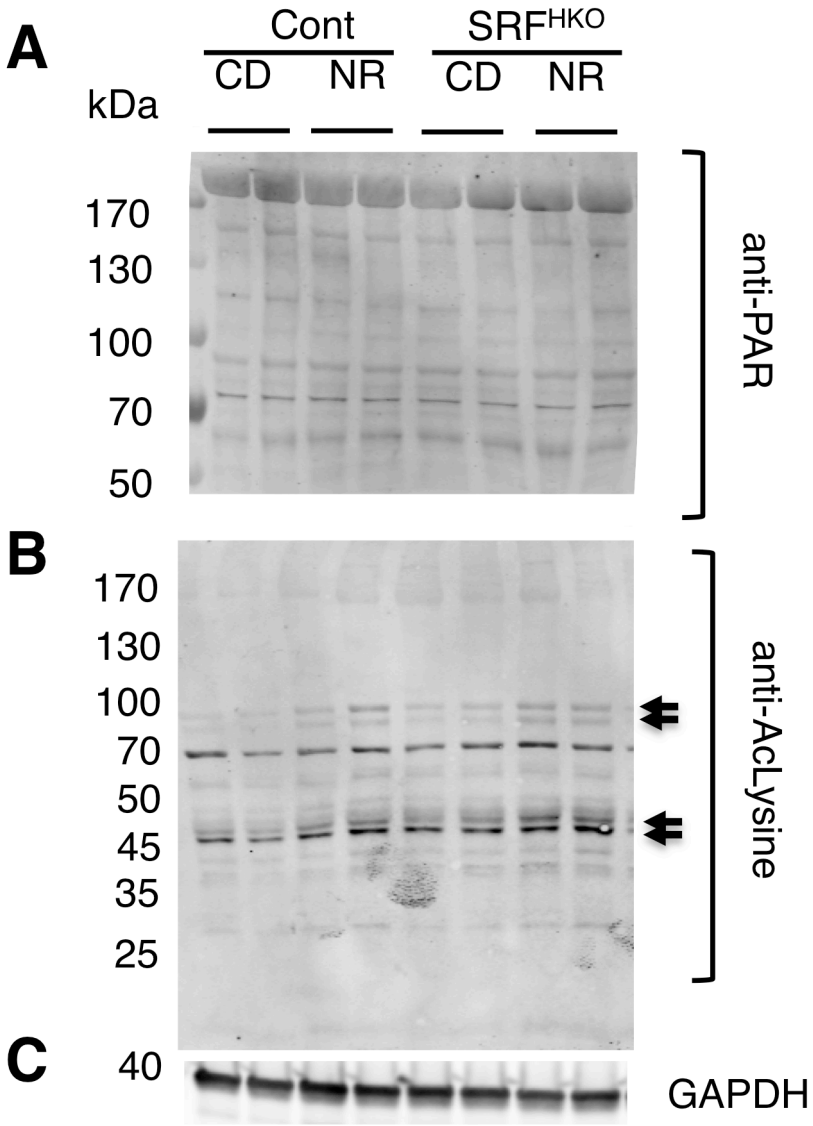

Figure IV. Acetylation and parylation level of cardiac proteins
Equal quantities of cardiac proteins from control and SRFHKO mice fed with regular diet (CD or NR enriched diet were extracted at D45 and analyzed by SDS-PAGE.
(A) Western blot analysis using an anti-PAR antibody
(B) Western blot analysis using an anti-acetyl-Lysine antibody. Arrows on the right points to bands whose signal is increased in NR-fed animals compared to CD diet.
(C) Western blot for GAPDH is shown as a loading control.

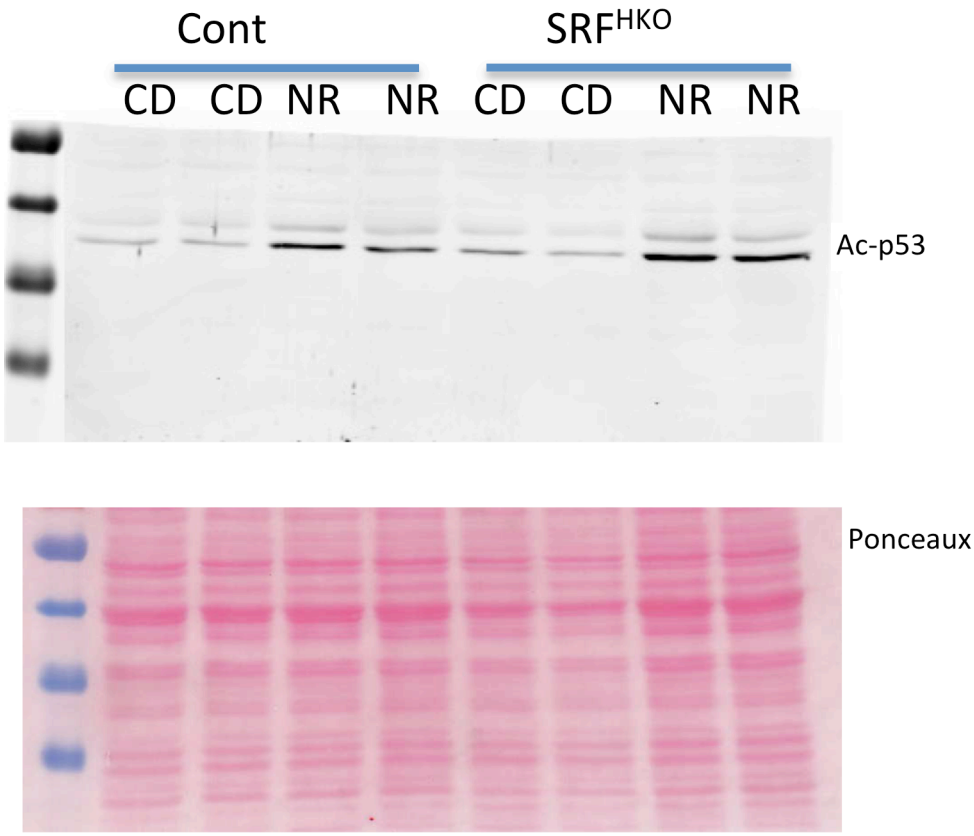

Figure V. Western blot analysis for Acetyl-p53 protein in cardiac extracts from control and and SRF^{HKO} mice fed with control CD diet or NR-diet.
Top: anti-acetyl p53 immunoblot. Bottom: Ponceau staining is shown for loading control

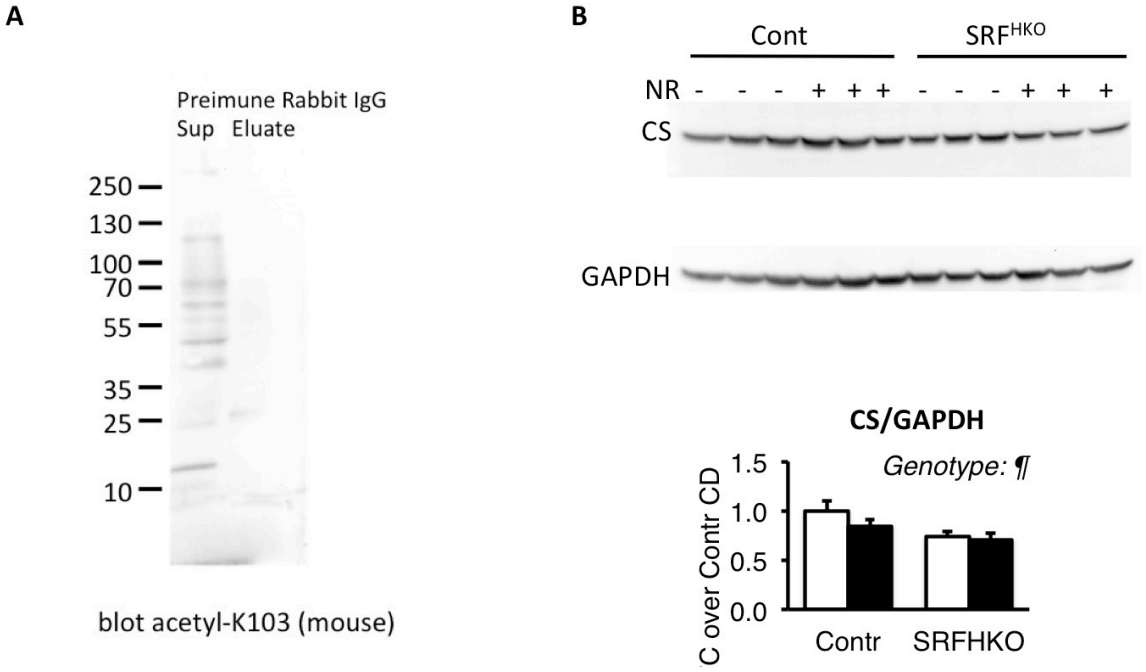

Figure VI. Western blot analysis for mitochondrial proteins in cardiac extracts from control and SRF^{HKO} mice fed with control CD diet or NR-diet. (A) Mouse anti-Acetyl-Lysine (K103) immunoblot of supernatant and eluate of immunoprecipitated cardiac protein extract with preiimmune rabbit IgG.

(B) Citrate synthase immunoblot. N=3 for each group. Right graphs show quantification performed with Image J software following the background substraction method. Two-way factorial ANOVA for independent samples. ¶ $p \leq 0.05$ for the genotype effect.

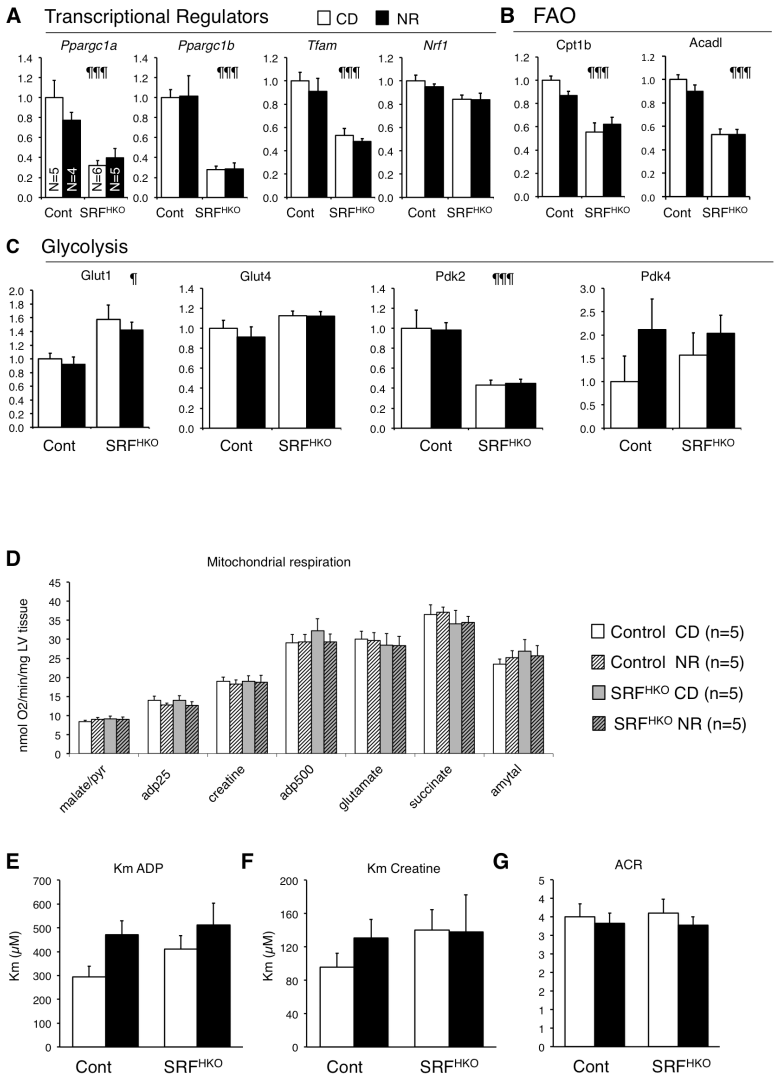

Figure VII. Impact of NR on genes involved in energy metabolism and mitochondrial respiration in permeabilized fibers.

LV tissue were harvested in control and SRF^{HKO} mice fed with regular chow diet (CD) or NR from D5 to day 45 and split for RTqPCR analysis or isolation of cardiac fibers for respiration studies (Figure 3 and S3). **(A-C)** RT qPCR analysis of transcriptional regulators of energy metabolism (**A**). Genes involved fatty acid beta-oxidation (**B**) and glycolysis (**C**). **(D-G)** Cardiac fibers were isolated from adults LV 45 days after tamoxifen injection in control and SRF^{HKO} mice fed with regular chow diet (CD) or NR enriched diet (NR) in the same series of mice than shown in Figure 3R-U. **(D)** Rate of mitochondrial oxygen consumption in permeabilized cardiac fibers using a Clarke electrodes after successive addition of indicated substrates. Individual samples were analyzed in triplicates (n=5 individuals for each group). **(E)** Km ADP. **(F)** Km Creatine. **(G)** Acceptor control ratio for ADP (ACR). Two-way factorial ANOVA for independent samples. ¶ $p \leq 0.05$, ¶¶¶ $p \leq 0.001$ for the genotype effect.

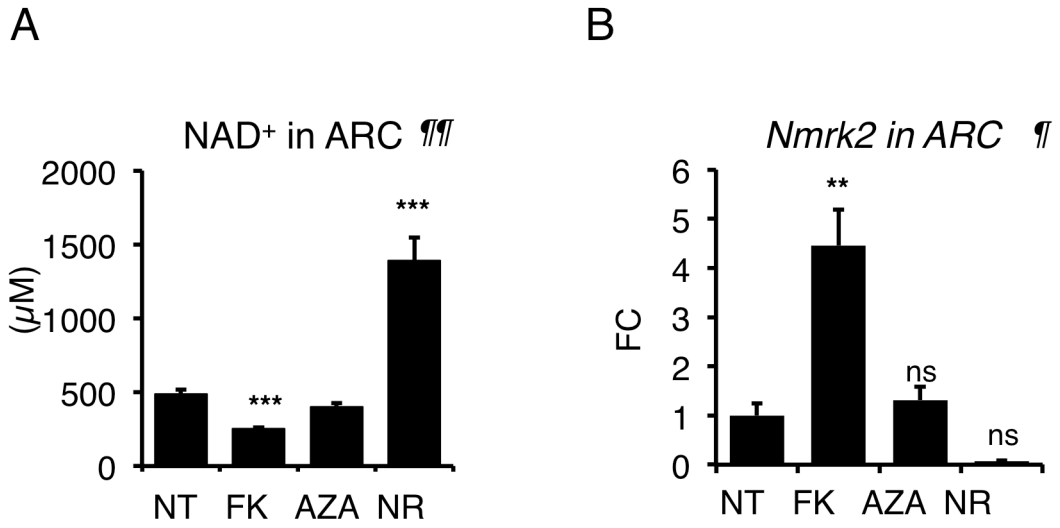

Figure VIII. NR impact in adult rat cardiomyocytes. NAD (**A**) and Nmrk2 mRNA (**B**) levels in adult rat cardiomyocytes (ARC). ARC were treated with 10 µM FK866, 20 µM azaserin or 1 mM NR for 65 h. NAD (NAD^+ + NADH) was extracted by the boiling buffered ethanol method. Data are given as µM concentration in cells using an average 30 pl cellular volume¶, ¶¶: One-Way ANOVA statistic $p< 0.05$, and $p<0.01$, respectively. **, ***, $p< 0.01$ and < 0.001, respectively for post-hoc Tukey test between any group versus NT control cells; ns non-significant.

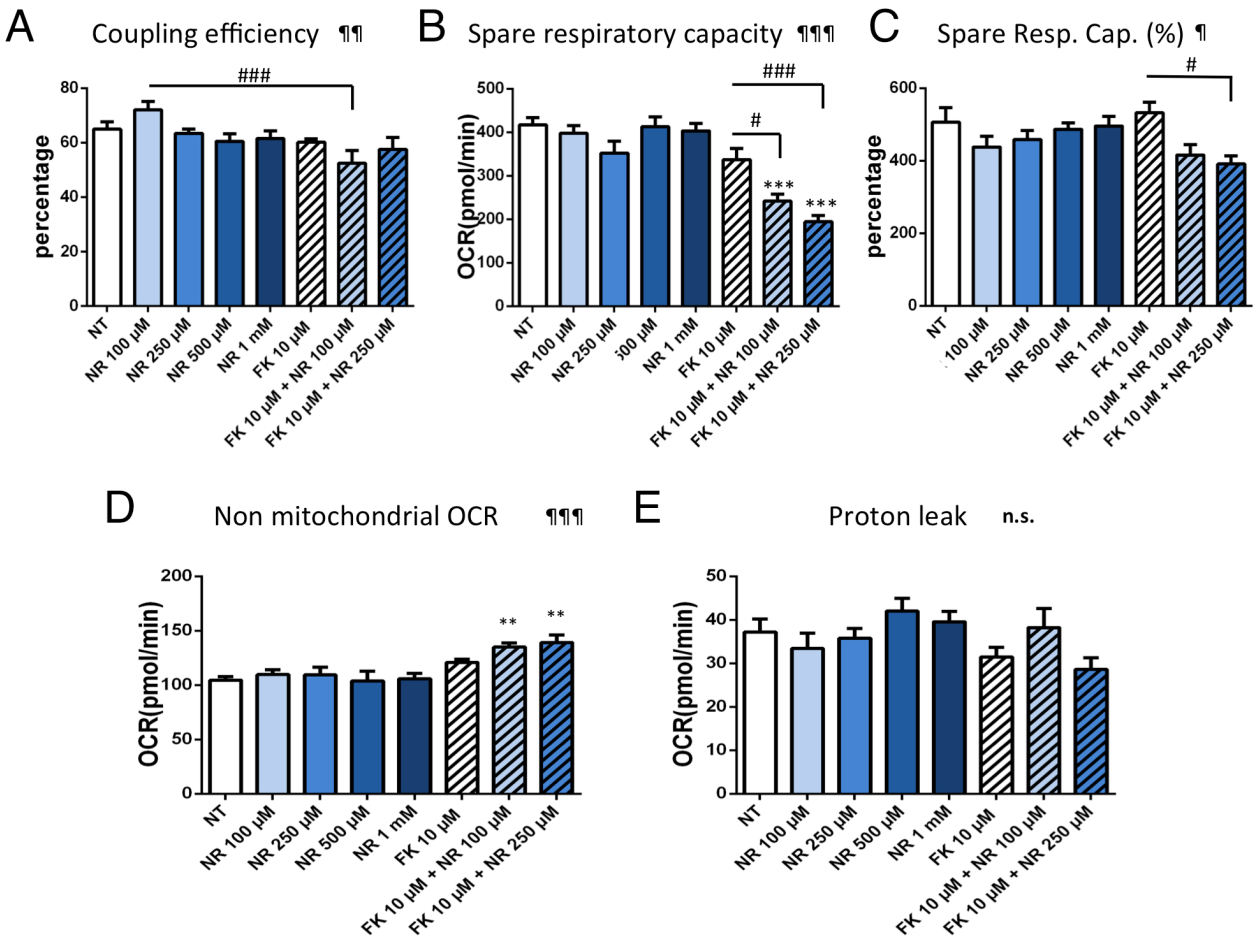

Figure IX. Impact of NR on NRC oxygen consumption rates following mitochondrial stress protocol. This figure complements Figure 4 of the main manuscript. NRC grown on Seahorse 96 well plates were analyzed at day 8 after 5 days of treatment**. (A)** Coupling efficiency is measured as (ATP Production Rate) / (Basal Respiration Rate). **(B)** Spare respiratory capacity is (Maximal Respiration) – (Basal Respiration). **(C)** Spare respiratory capacity as a % is defined as (Maximal Respiration) / (Basal Respiration). **(D)** Non mitochondrial oxygen consumption rate is the minimum rate measurement after inhibition of respiration with rotenone and antimycin A. **(E)** Proton leak is calculated as the (minimum rate measurement after Oligomycin) – (non-mitochondrial respiration). N= 10 for each group. ¶, ¶¶, ¶¶¶: One-Way ANOVA statistic p< 0.05, <0.01 and < 0.001, respectively. **, ***, p< 0.01 and < 0.001, respectively for post-hoc Tukey test between any group versus NT control cells. #, ###, p < 0.05, and < 0.001, respectively for post-hoc Tukey test for other comparisons, notably NR 100 µM versus FK866 10 µM + NR 100 µM and FK 10 µM versus FK866 10 µM + NR 250 µM.